Terr. Atmos. Ocean. Sci., Vol. 30, No. 5, 649-674, Ocober 2019 doi: 10.3319/TAO.2019.07.07.01

Gas plumes and near-seafloor bottom current speeds of the southernmost Okinawa Trough determined from echo sounders

Ching-Hui Tsai[1], Shu-Kun Hsu[1, 2, *], Yen-Fu Chen[2], Hsiao-Shan Lin[1], Shiou-Ya Wang[1], Song-Chuen Chen[3], Chin-Wei Liang[1], and Yen-Yu Cho[1]

[1] *Center for Environmental Studies, National Central University, Taoyuan City, Taiwan*
[2] *Department of Earth Sciences, National Central University, Taoyuan City, Taiwan*
[3] *Central Geological Survey, Ministry of Economic Affairs, Taipei City, Taiwan*

Article history:
Received 26 January 2019
Revised 2 July 2019
Accepted 7 July 2019

Keywords:
Gas plume, Bottom current, Okinawa Trough, Echo sounder

Citation:
Tsai, C.-H., S.-K. Hsu, Y.-F. Chen, H.-S. Lin, S.-Y. Wang, S.-C. Chen, C.-W. Liang, and Y.-Y. Cho, 2019: Gas plumes and near-seafloor bottom current speeds of the southernmost Okinawa Trough determined from echo sounders. Terr. Atmos. Ocean. Sci., 30, 649-674, doi: 10.3319/TAO.2019.07.07.01

ABSTRACT

Using echo sounders to detect gas plumes in seawater is common, especially in the context of hydrothermal circulation areas or gas hydrate-bearing cold seeps. To understand the distribution of gas plumes in the southernmost Okinawa Trough, we have conducted 13 cruises with a 38 kHz single-beam echo sounder (EK60). A total of 266 gas plumes of acoustic image, associated with the hydrothermal circulation, are detected. To estimate the near-seafloor bottom current speeds, 201 gas plumes are further used. As a result, the gas plumes around the axial depression of the Okinawa Trough generally tilt to the northeast at rising tides and high tides, suggesting a northeastward flow of the bottom current. However, the gas plumes in the Keelung continental slope tilt to the southwest at ebb tides and low tides, suggesting a southwestward flow of the bottom current. Our results significantly show a good estimation of the near-seafloor bottom currents from EK plume images in the case of lacking real observations. The directions of the bottom currents depend on semi-diurnal tides. Assuming a quasi-constant speed of upward gas bubbles out of seabed, we have estimated the bottom current speeds in 6 hydrothermal circulation zones near the rifting center of the southernmost Okinawa Trough. The estimated bottom current speeds in submarine volcanic areas vary largely from 2 to 160 cm s^{-1}, but bottom current speeds in relatively flat region are between 20 and 50 cm s^{-1}. The large variation of the bottom current speeds in the submarine volcanic areas could be due to the variable emissions of the gases out of the submarine volcanic areas.

1. INTRODUCTION

Relative to the Eurasian Plate, the Philippine Sea Plate moves northwestward at a speed of ~8 cm yr^{-1} around Taiwan (Seno et al. 1993; Yu et al. 1997). The Philippine Sea Plate is subducting beneath the Eurasian Plate and has formed the Ryukyu subduction zone (Letouzey and Kimura 1985; Sibuet et al. 1987). Okinawa Trough is an active back-arc basin behind the Ryukyu Arc (Uyeda 1977; Lee et al. 1980; Kimura 1985; Sibuet et al. 1987) (Fig. 1). Our study area is located in the southernmost Okinawa Trough. Morphologically, Keelung Valley and Mienhua Canyon are loacated in the northern margin of the Okinawa Trough and transport sediments from the East China Sea to the Okinawa Trough (Hsu et al. 1996). The current rifting of the southern Okinawa Trough area could start at 0.1 million years ago (Sibuet et al. 1998).

Kimura et al. (1986, 1988) and Shyu and Liu (2001) have pointed out unusually high geothermal flows in the Okinawa Trough, especially some hydrothermal hillocks and biota. It reveals an actively hydrothermal circulation system in the Okinawa Trough. Earthquakes and active submarine volcanoes are common in the southernmost Okinawa Trough (Lin et al. 2007, 2009). It suggests intensively magma activity associated with abundant submarine volcanoes. Base on the multi-beam bathymetric data from the ACT cruise of the Taiwan-French cooperation in 1996 (Lallemand et al. 1997), there are more than 70 submarine volcanoes in the southernmost area of the Okinawa Trough

* *Corresponding author*
E-mail: hsu@ncu.edu.tw

(Fig. 2). Hydrothermal circulations are linked to the activities of the submarine volcanoes (Massoth et al. 1988). In a hydrothermal circulation area, volcanic materials are carried by hot water to form a smoky zone (Baker et al. 1995), creating a "Black Smoker" feature, which provides an important conduit for the exchange of seawater and crustal metals.

Because of a hydrothermal circulation, volcanic material could be carried by hot water and form a relatively turbid area in the seawater. Using a 38 kHz single-beam echo sounder, German et al. (1994) have observed the hydrothermal circulation phenomenon of the mid-ocean ridge in the northeastern Pacific Ocean. Similarly, Tsai (1999) and Lee (2005) also have observed a hydrothermal circulation system in the southernmost of the Okinawa Trough; 12 active hydrothermal areas were discovered (Lee 2005). A 38 kHz single-beam echo sounder has also been used to observe cold seep systems associated with gas hydrates. For example, the researches on gas hydrates in the Black Sea (Polikarpov et al. 1989; Naudts et al. 2006), Hydrate Ridge (Heeschen et al. 2003), and the southwestern Taiwan (Chen et al. 2010; Hsu et al. 2018). However, it is remarkable that several acoustic images of the gas plumes in water columns have been tilted, instead of a vertical ascent. Veloso et al. (2015) used three typical examples of plumes image from single-beam echo sounders to explain how a near-seafloor bottom current could affect rising bubbles from a seabed. The application of multi-beam echo sounder water-column imaging technology allows us to understand the relationship between the shape of the plume shape and the direction of current in the seawater (Urban et al. 2017). Additionally, the mooring observation on the hydrothermal mounds of the mid-ocean ridge (Fujioka et al. 1997) and the ADCP (Acoustic Doppler Current Profiler) observation in the Hatoma Knoll hydrothermal field of the southern Okinawa Trough (Furushima and Yamamoto 2015) have shown that the fluctuation cycle of temperature, pressure, and current is synchronized with semidiurnal tides.

In this study, we will analyze the EK60 acoustic images from 13 surveys in the southernmost Okinawa Trough (Fig. 3), with the purpose of better understanding the gas plumes distribution and the relationship between the gas plumes images and the near-seafloor bottom current in the southernmost Okinawa Trough. As mentioned previously, gas plume locations could be excellent sites for the exchange of seawater and crustal metals; thus, bottom current directions may be used to indicate the probable precipitation areas of metalliferous sediments.

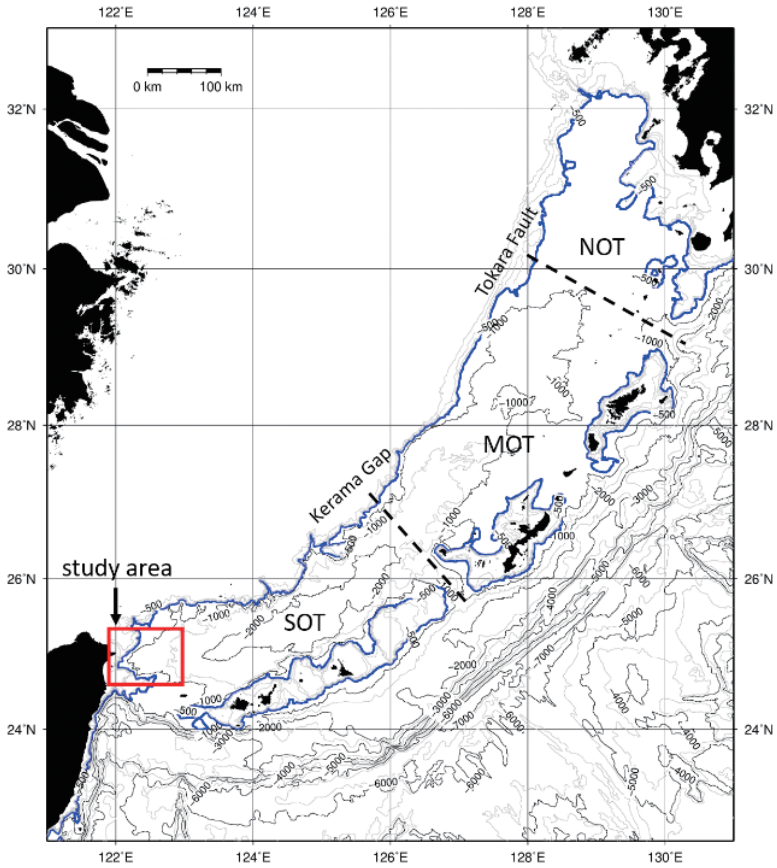

Fig. 1. Bathymetry Bathymetric map of the Okinawa Trough between Taiwan and Japan. The regional map of the Okinawa Trough, which could be separated into three portions. They are the Northern Okinawa Trough (NOT), the Middle Okinawa Trough (MOT), and the Southern Okinawa Trough (SOT), separated by the Kerama Gap and the Tokara Fault respectively. This study area is located in the westernmost OT.

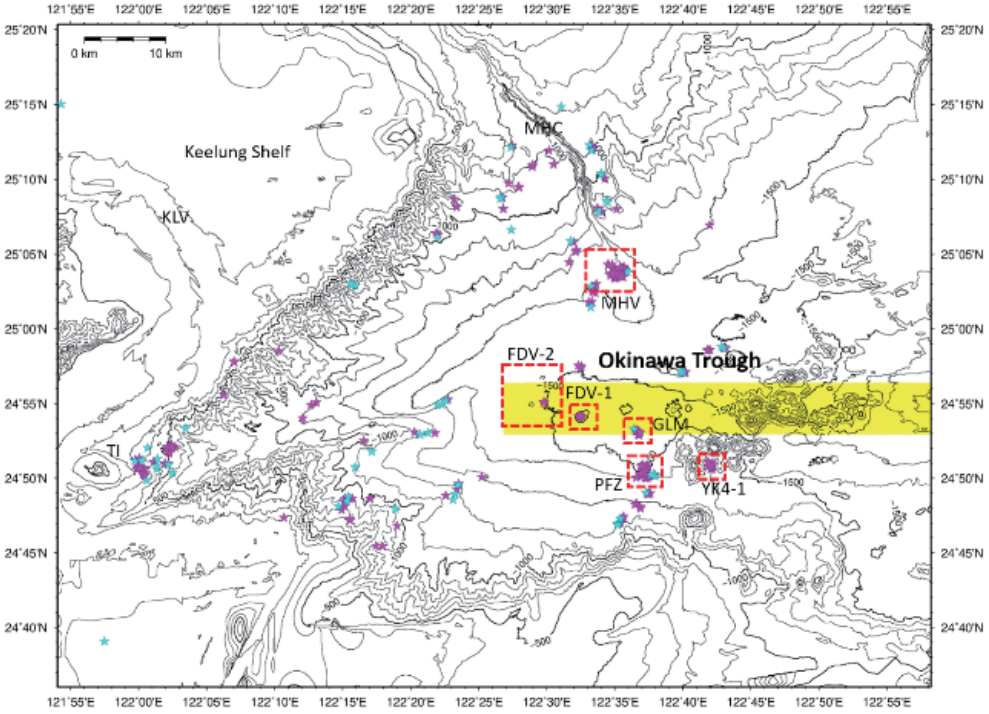

Fig. 2. Topography of the study area. The main features include the southernmost Okinawa Trough back-arc basin, the Keelung Valley (KLV), the Turtle Island (TI), and the Mienhua Canyon (MHC). The stars indicate the locations of the 266 gas plumes. The pink stars indicate the locations of 201 complete plume images and the light blue stars indicate the locations of 65 incomplete gas plume images. The red boxes indicate 6 active hydrothermal circulation zones and 11 gas plume images used to estimate the near-seafloor bottom current velocities. The yellow zone indicates the axial portion of the Okinawa Trough.

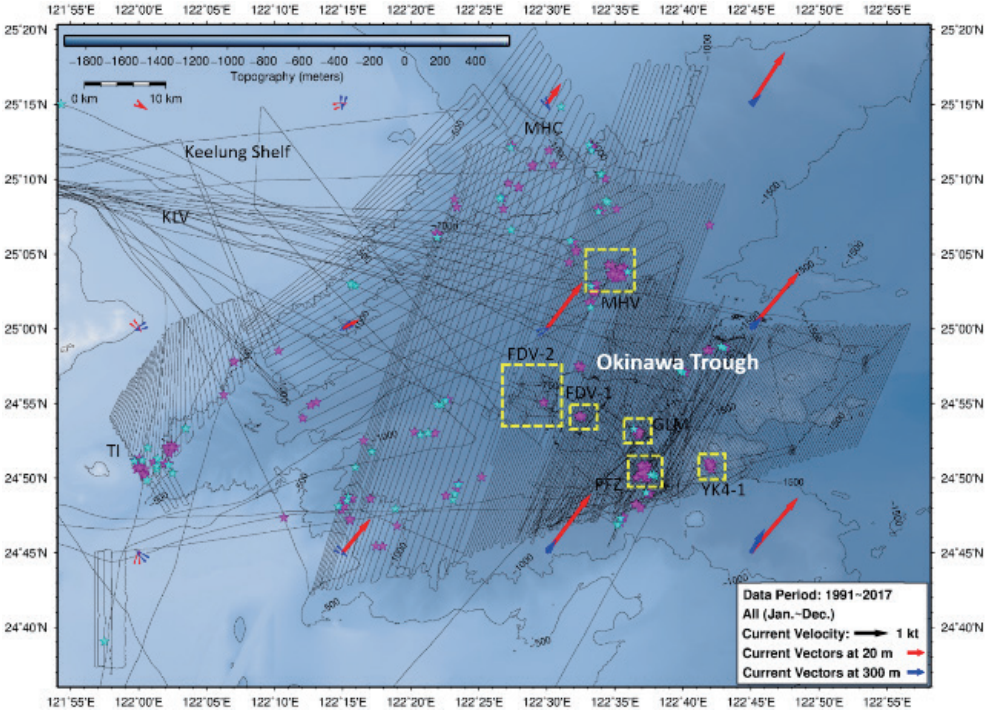

Fig. 3. The ship-tracks of 13 surveys used in this study. The ship-tracks mainly show NE-SW orientation. The data covers the areas of southernmost Okinawa Trough, the Keelung Shelf slope and the northeast side of the Turtle Island. Based on the Ocean Data Bank, the currents at 20 - 300 m deep in the study area are dominated by the northeast flow. The yellow boxes indicate same locations as in Fig. 2.

2. DATA COLLECTION AND PROCESSING

The bathymetric data used in this study were collected during 13 cruises from 2014 to 2018 with EK60 scientific single-beam sounder, which uses the split beams technology and two frequencies (38 and 120 kHz). Because the water depths in our study area are generally deeper than 500 m (Fig. 3), we only use the 38 kHz. The transducer has a 7° beam width. Post-processing of data is done with the FM-Midwater tool in the Fledermaus software suite, so that the gas plume images and the adjustment of energy were obtained.

Based on the existing data of physical oceanography for the water depth as deep as 300 m (Ocean Data Bank of the Ministry of Science and Technology, Taiwan, R.O.C.), the annual average current flow has a stable northeast flow in the shallow part to the east of 122°20'E. The current flow becomes faster eastward (Fig. 3). To the west of 122°20'E, morphologically the area belongs to the Keelung continental shelf and slope. It has a slower velocity of flow and inconsistent flow direction; especially the flow direction is quite unstable at a water depth of 300 m (Fig. 3). In any case, there is a lack of current velocity information for the water depths greater than 300 m.

Among our 13 cruises, there are 3 deep-tow sonar surveys with a ship speed of ~2 knots and 10 multi-beam echosounder cruises with a ship speed of ~6 knots. Based on our EK60 data in the southernmost Okinawa Trough, we have identified 266 gas plumes (Figs. 2 and 3 and Appendix A). According to Veloso et al. (2015), the relationship of a gas plume image to a bottom current could have 3 cases: (1) current from the opposite direction of the ship's movement, (2) current from the same direction as the ship's movement, and (3) current oblique to the ship's movement. In the second case, a most complete and clear plume image can be imaged. Because a gas plume image in the third case is obliquely obtained by cutting across the gas plume, the plume image near the seabed is usually missed. In consequence, the portion of the gas plume image could be mistaken for a school of fish in the seawater. Therefore, based on the completeness of our 266 gas plume images, we separated 201 complete images of gas plume (remark A in Appendix A) from 65 incomplete images (remark B in Appendix A). Figures 4 to 16 display the 201 complete images of gas plume that will be further analyzed in this study.

3. RESULTS AND DISCUSSION

3.1 Gas Plumes and Hydrothermal Circulation

During our 3 deep-tow sonar surveys, sidescan sonar data (120 and 410 kHz) were collected. Active gas plumes (emitting gas bubbles) associated with hydrothermal circulation can be clearly observed in the sidescan sonar images (Figs. 4 and 5). As shown in the sidescan sonar images of Fig. 5, gaseous bubbles or materials carried by hot water have escaped from chimneys or mounds (Hsu 2017). Those gas plumes imaged in the sidescan sonar can also be imaged in the 38 kHz single beam sonar (EK60) (Figs. 4 and 5). The gas plume heights are generally around 350 m, but can be as high as 800 m.

3.2 Gas Plumes and Tidal Variation

Crone et al. (2010) indicated that tidal variation could affect current velocity near a hydrothermal vent. Chemical concentrations and temperatures of a current may also be changed (Larson et al. 2007). For example, Veirs et al. (2006) showed that the semi-diurnal tide affects the tidal oscillations of ocean currents around the Grotto mound in the Juan de Fuca Ridge region. Semi-diurnal tides also affect the deep ocean around the mid-Atlantic Ridge (Fujioka and Mitsuzawa 2001) and around the seabed near Oahu of Hawaii (Aucan et al. 2006). In addition, Berdeal (2006) found significant inertial oscillations in the time series of horizontal flow in an 11-month near-bottom ADCP observation; similar result was obtained in the southern Okinawa Trough (Furushima and Yamamoto 2015). It is concluded that a semi-diurnal tide will affect the current flow direction and flow rate in the seawater.

In our study area, the lower bound of the seawater thermocline is generally at 600 m deep and can be as deep as 800 m deep. Therefore, most of the seawater shallower than 600 m contains a fairly thick suspension layer. In consequence, most of the gas plumes in our study area can only be imaged clearly at the water depth deeper than 600 m. However, as imaged by the EK60, several gas plumes have a tilted tendency that could be associated with the bottom current (Figs. 4 to 16). In order to understand the gas plume tilt phenomenon, we compare the gas plume images with the tidal data. For that, we adopt the global ocean tide model NAO.99b (Matsumoto et al. 2000) and relate each gas plume image to the tidal variation at the same period of data acquisition. In Figs. 4 to 16, we use blue, red, yellow and green colors to mark the rising tide, ebb tide, high tide and low tide respectively.

As shown in Table 1, we have integrated the tilt directions of the EK60 plume images in Figs. 4 to 16 and different tidal conditions. Because EK60 is a single-beam detection system, the change of a gas plume image can only be observed along the ship track. Therefore, only the tilted gas plume images along the plane of the ship tracks (i.e., NE-SW orientation) are considered in this study. For that, the 201 plume images in Figs. 4 to 16 were collected when the ship's course was parallel to or against the current directions.

As shown in Fig. 11, the gas plume images from h21 to h33 in the middle portion of the southernmost Okinawa Trough indicate that the plume images incline to the northeast when the tides are rising or at high tides. At ebb tides

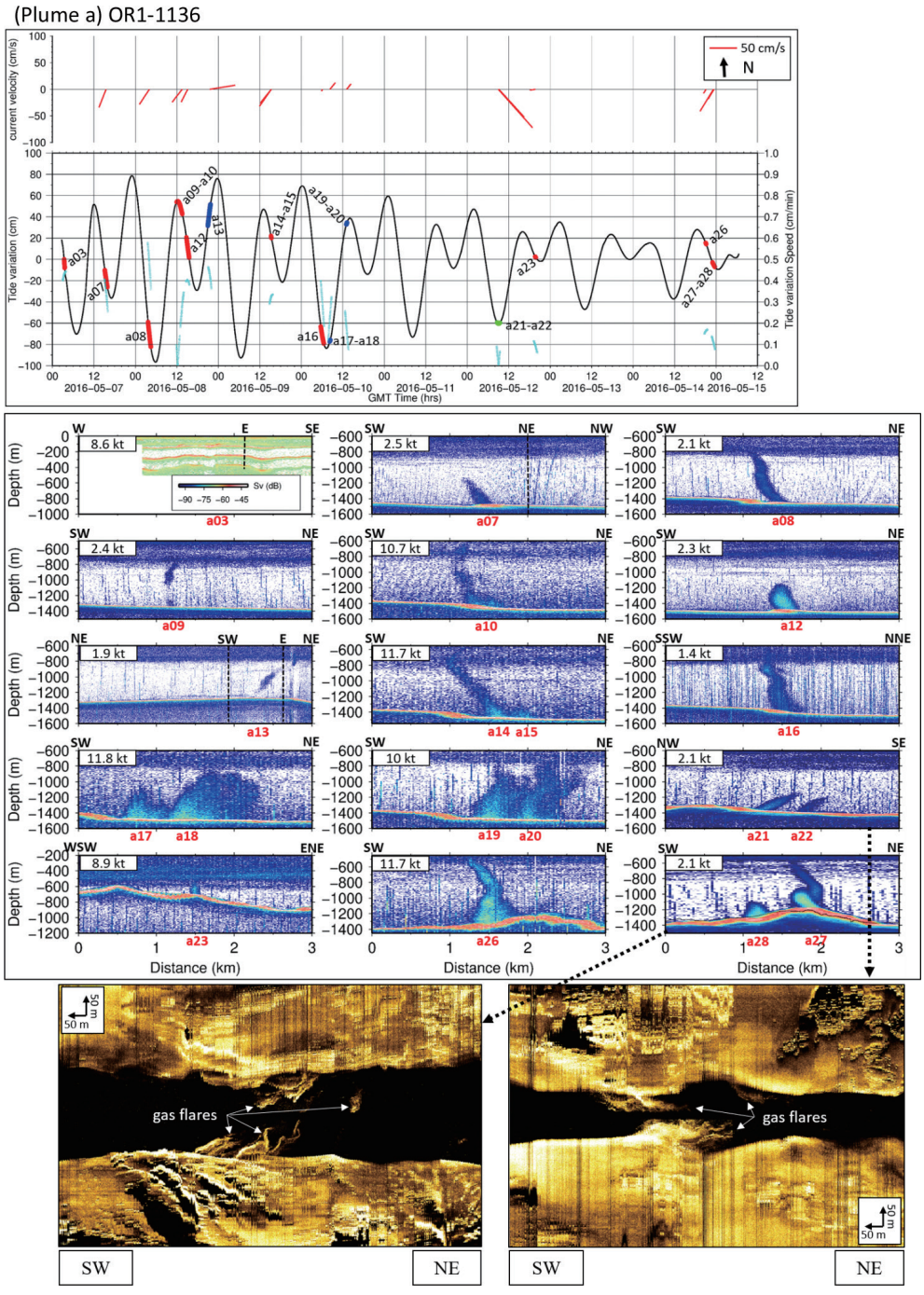

Fig. 4. EK60 images of the gas plumes of a-series. Each gas plume image is generally situated at the middle of each panel. The relatively tidal height of each plume is shown in the top panel. Four kinds of tidal situations are shown in different colors of blue, red, yellow, and green, which correspond to rising tide, ebb tide, high tide, and low tide, respectively. It is noted the plumes a21, a22, a27, and a28 have clear images in the water columns of deep-tow sidescan sonar data.

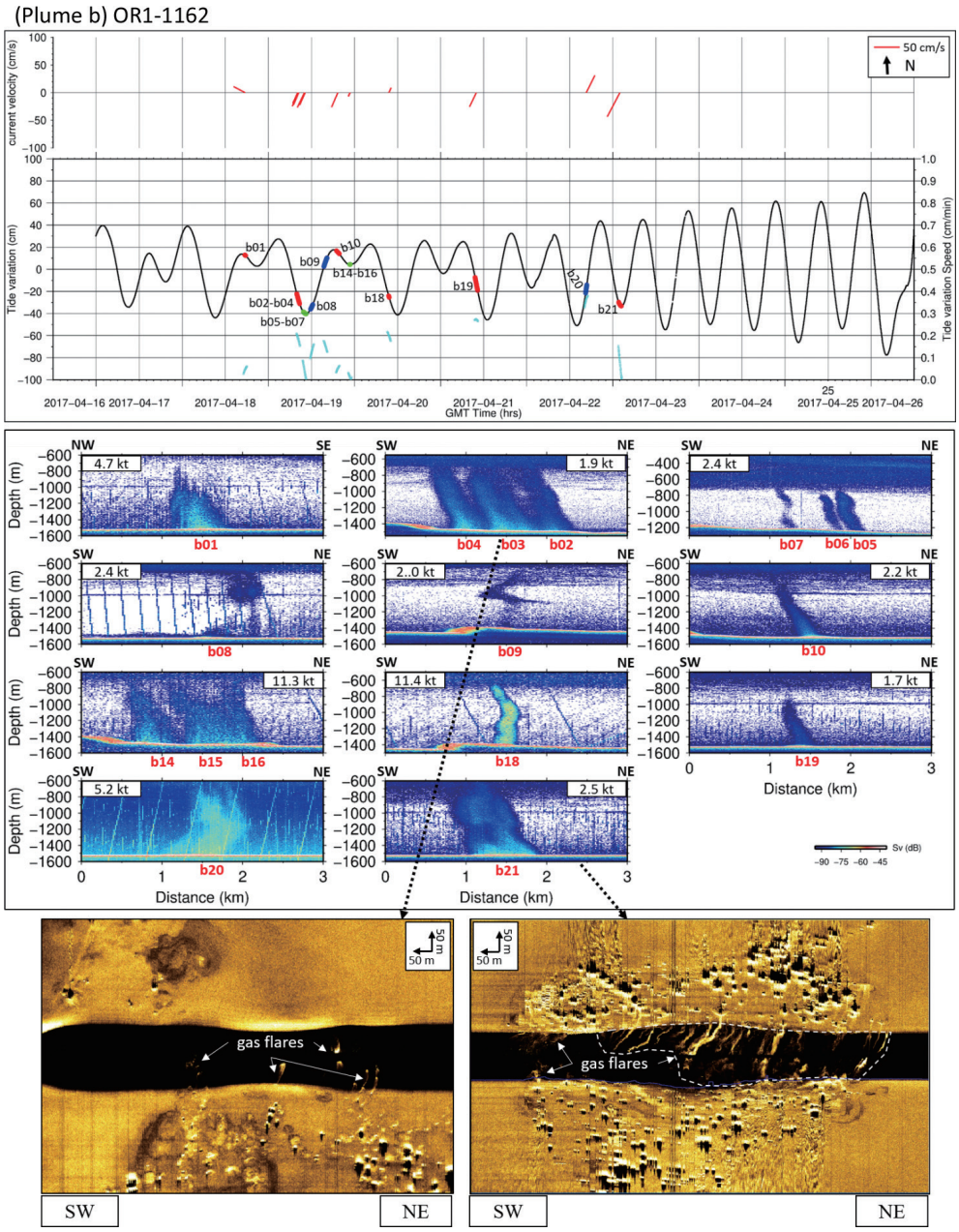

Fig. 5. EK60 images of the gas plumes of b-series. The relevant descriptions are shown in Fig. 4. The plumes b02 to b04 and b21 plumes have clear images in the water columns of deep-tow sidescan sonar data.

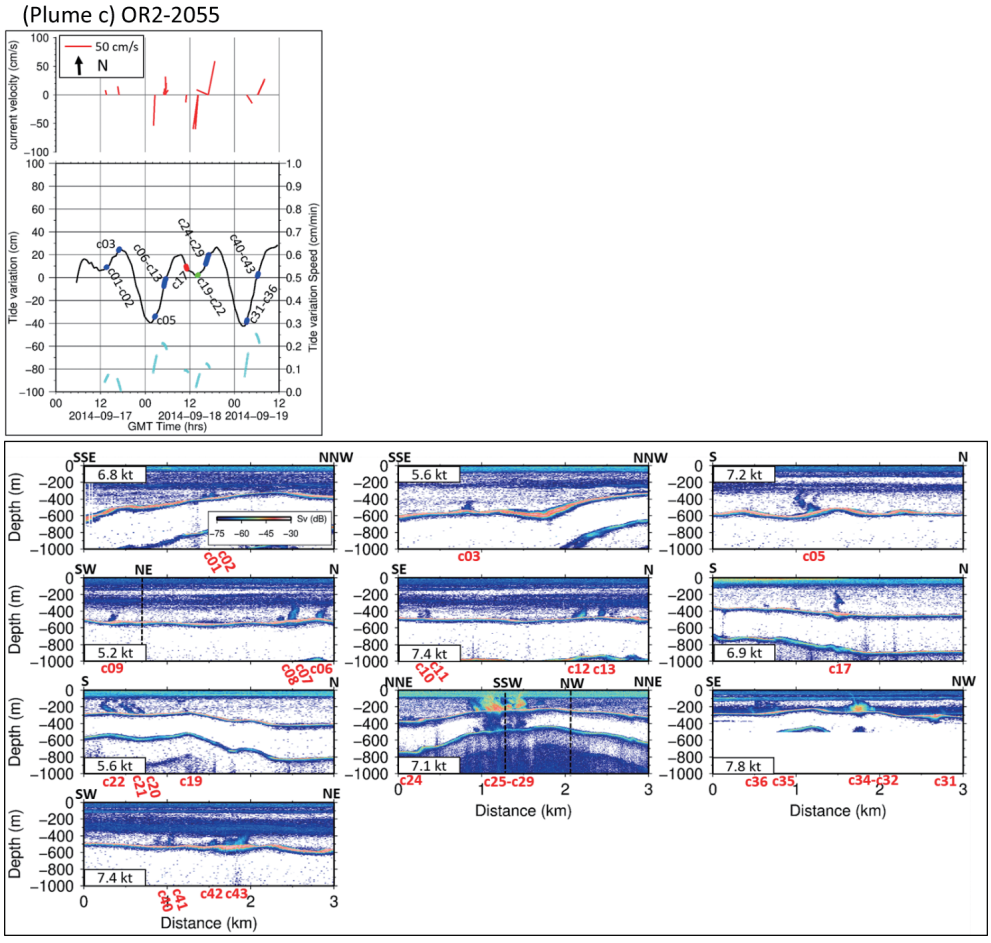

Fig. 6. EK60 images of the gas plumes of c-series. The relevant descriptions are shown in Fig. 4.

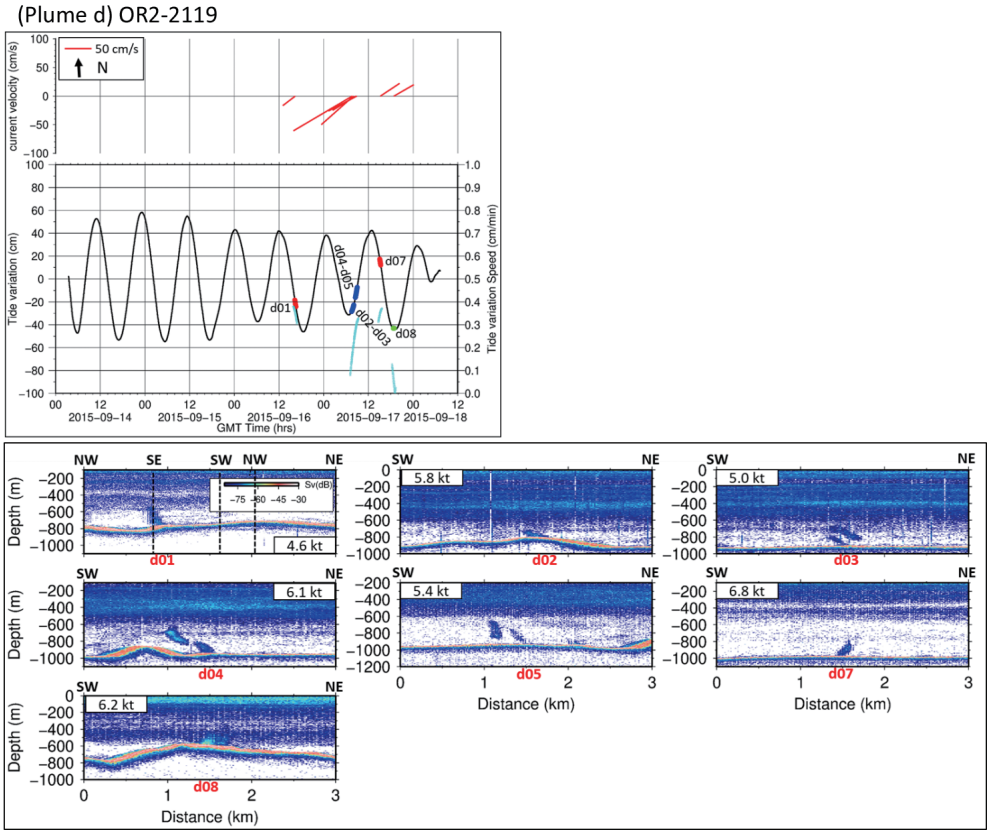

Fig. 7. EK60 images of the gas plumes of d-series. The relevant descriptions are shown in Fig. 4.

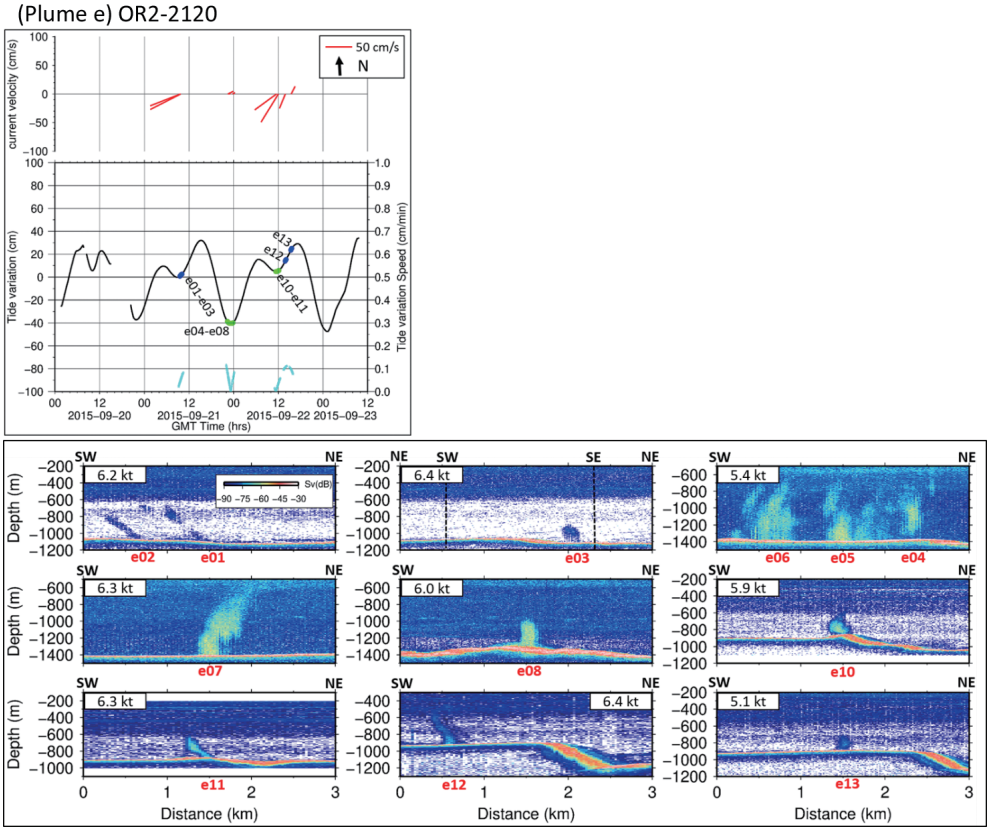

Fig. 8. EK60 images of the gas plumes of e-series. The relevant descriptions are shown in Fig. 4.

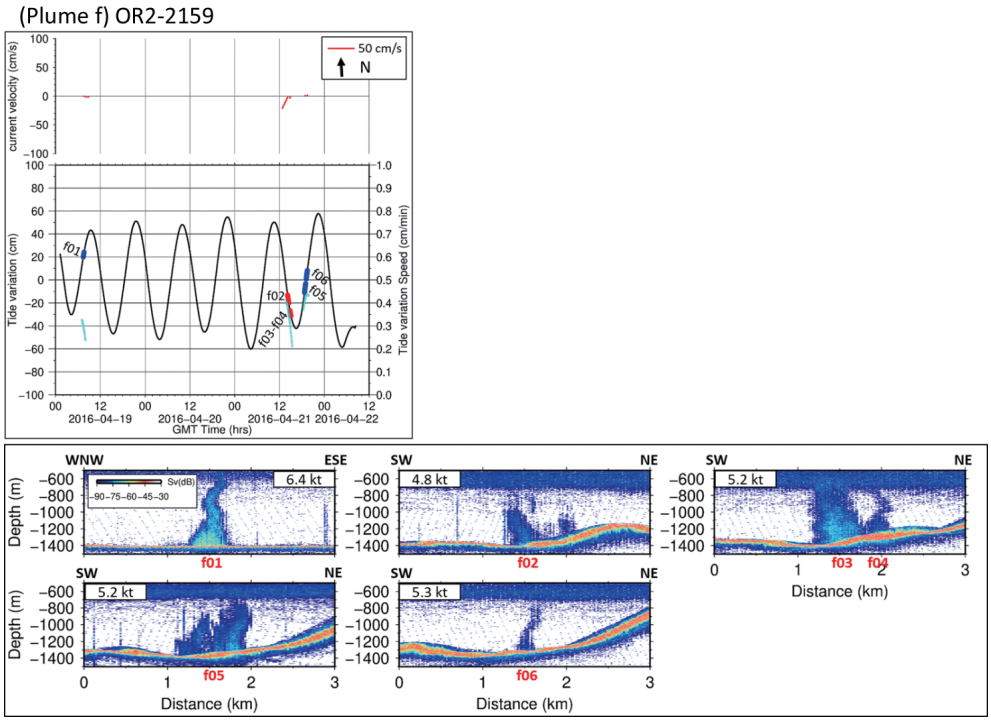

Fig. 9. EK60 images of the gas plumes of f-series. The relevant descriptions are shown in Fig. 4.

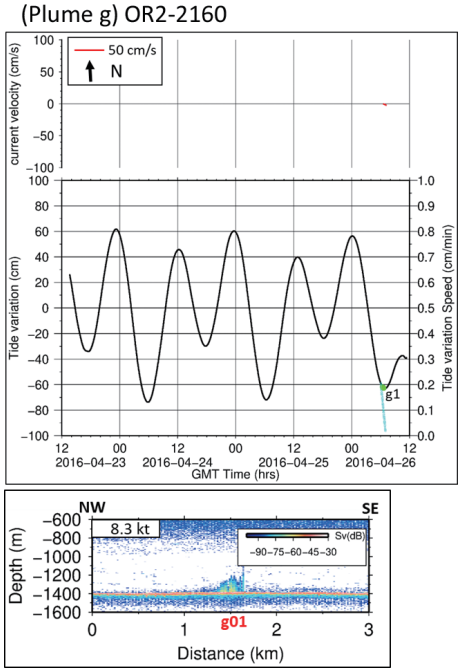

Fig. 10. EK60 image of the g01 gas plume. The relevant descriptions are shown in Fig. 4.

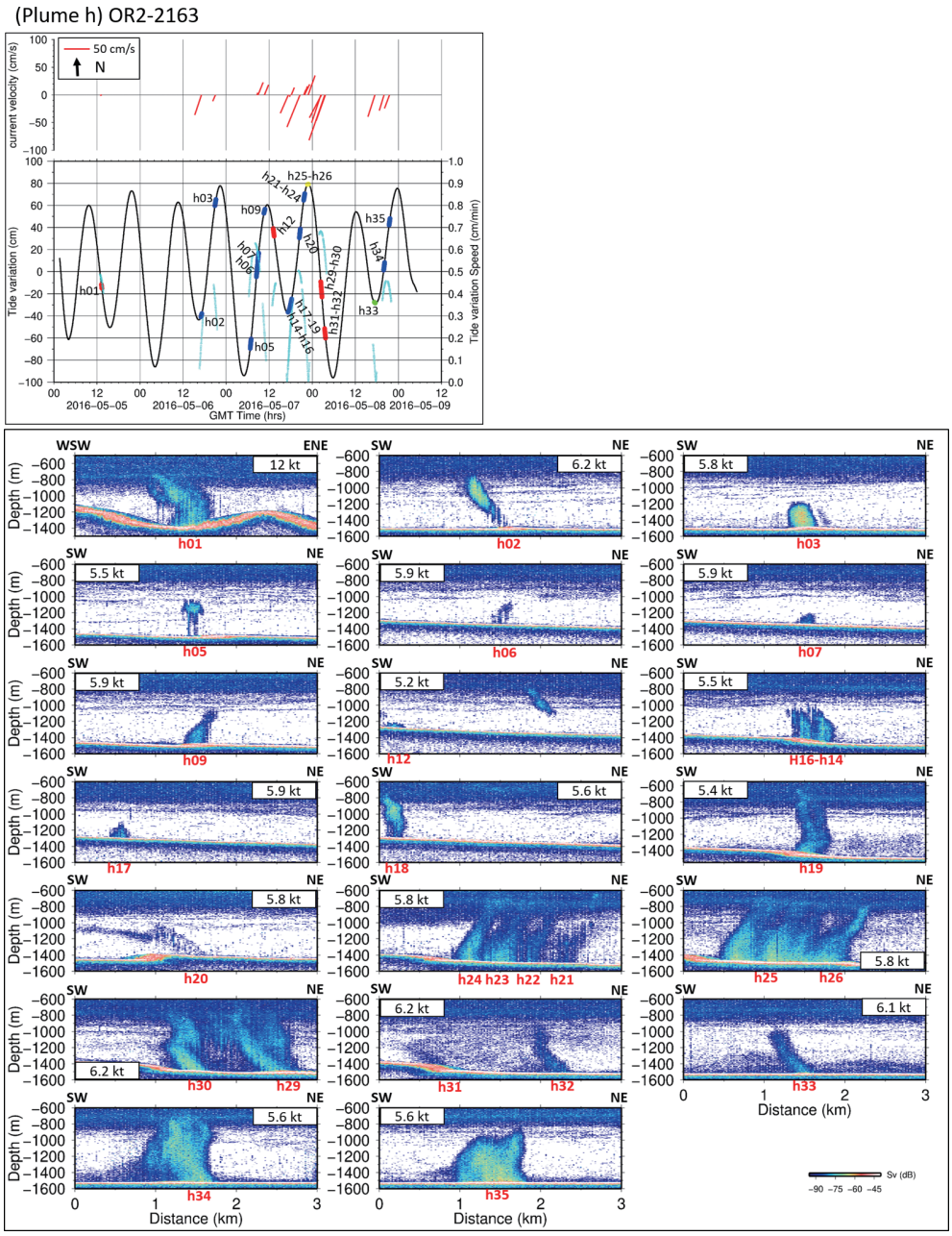

Fig. 11. EK60 images of the gas plumes of h-series. The relevant descriptions are shown in Fig. 4.

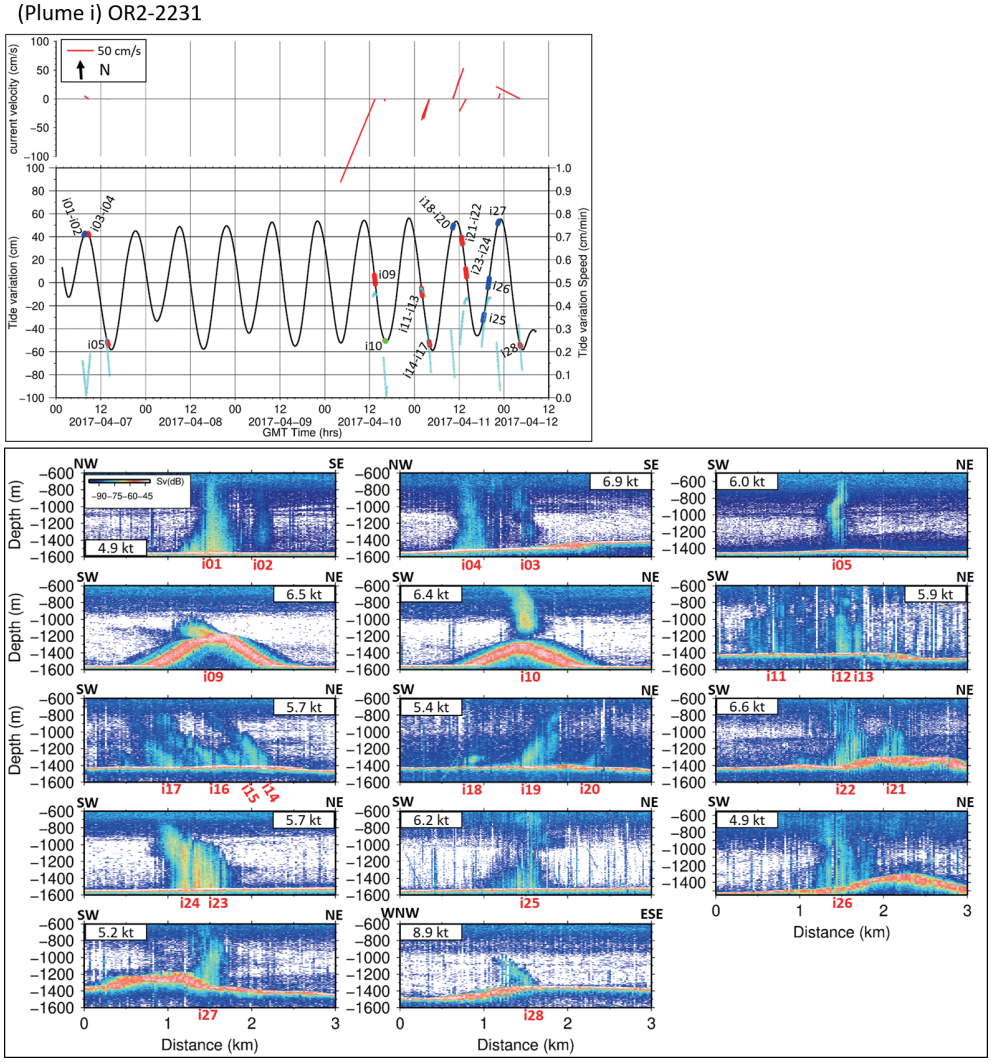

Fig. 12. EK60 images of the gas plumes of i-series. The relevant descriptions are shown in Fig. 4.

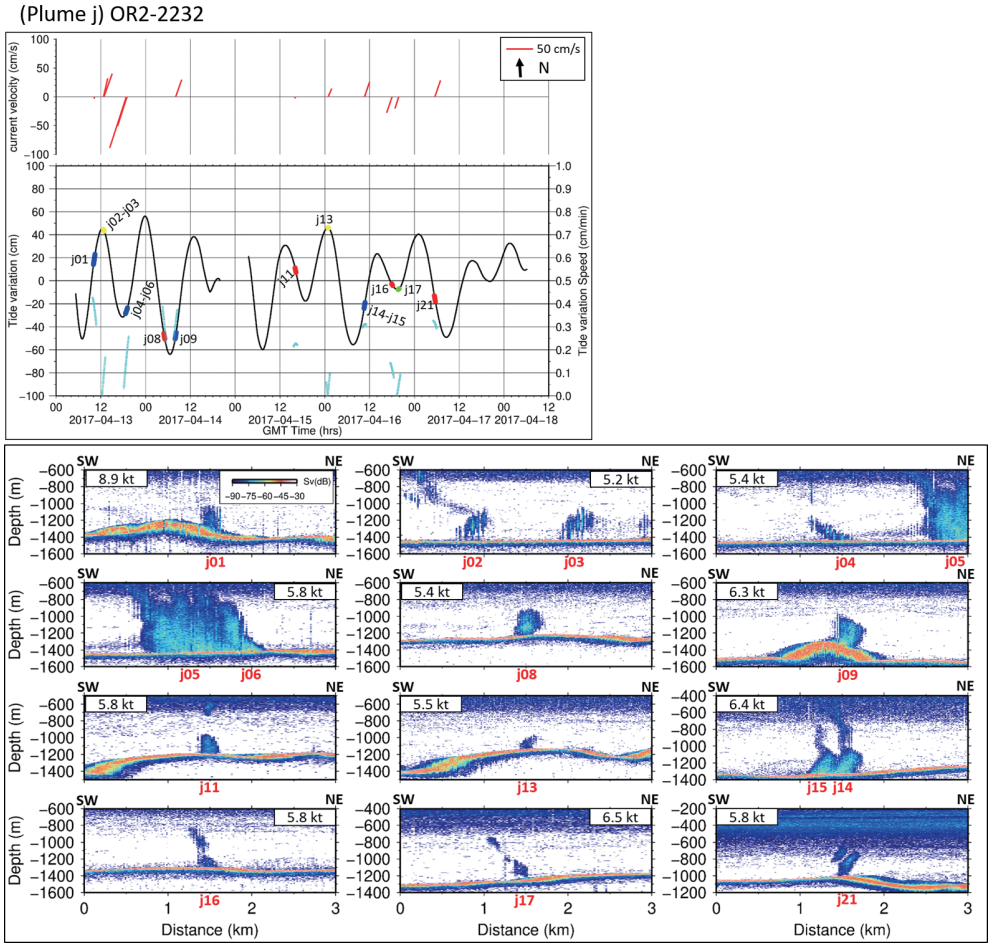

Fig. 13. EK60 images of the gas plumes of j-series. The relevant descriptions are shown in Fig. 4.

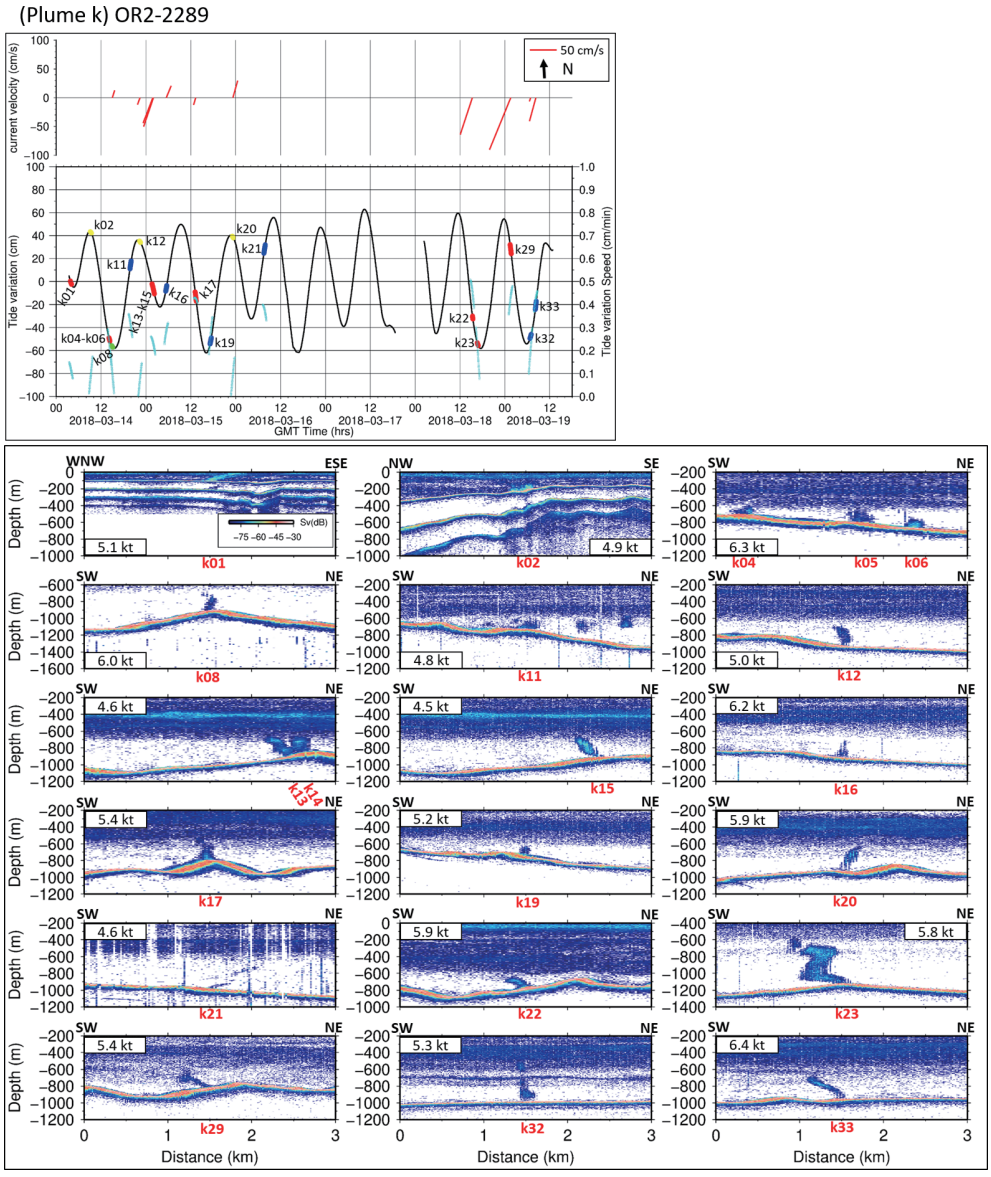

Fig. 14. EK60 images of the gas plumes of k-series. The relevant descriptions are shown in Fig. 4.

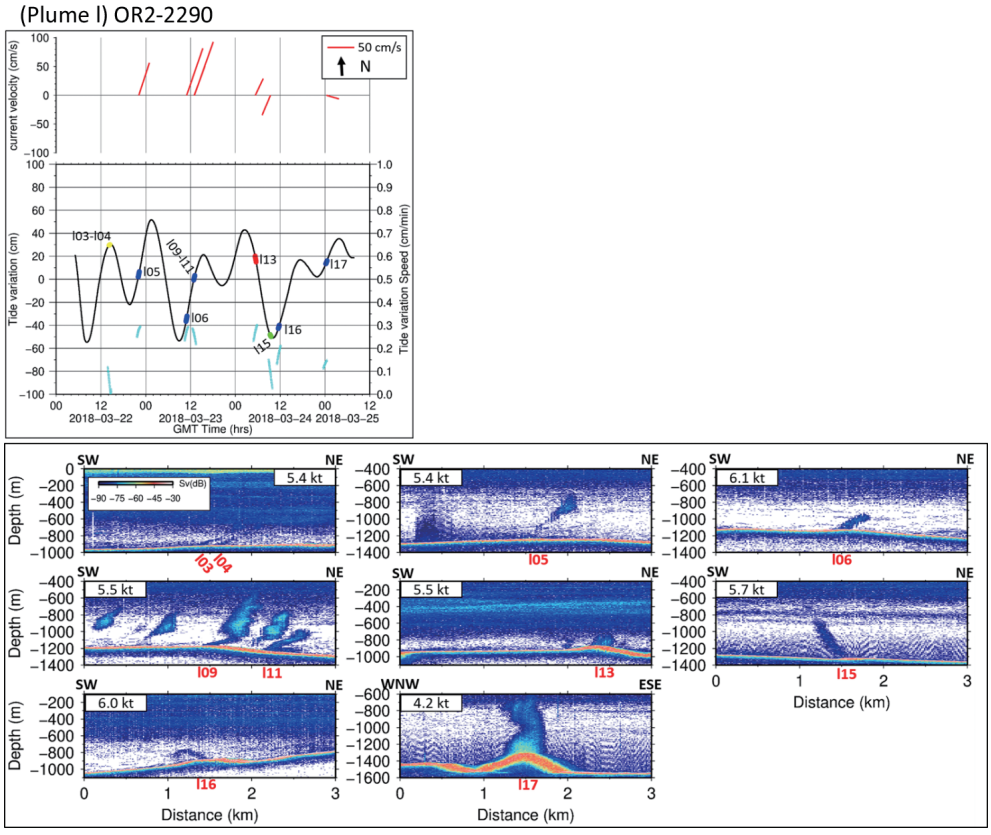

Fig. 15. EK60 images of the gas plumes of l-series. The relevant descriptions are shown in Fig. 4.

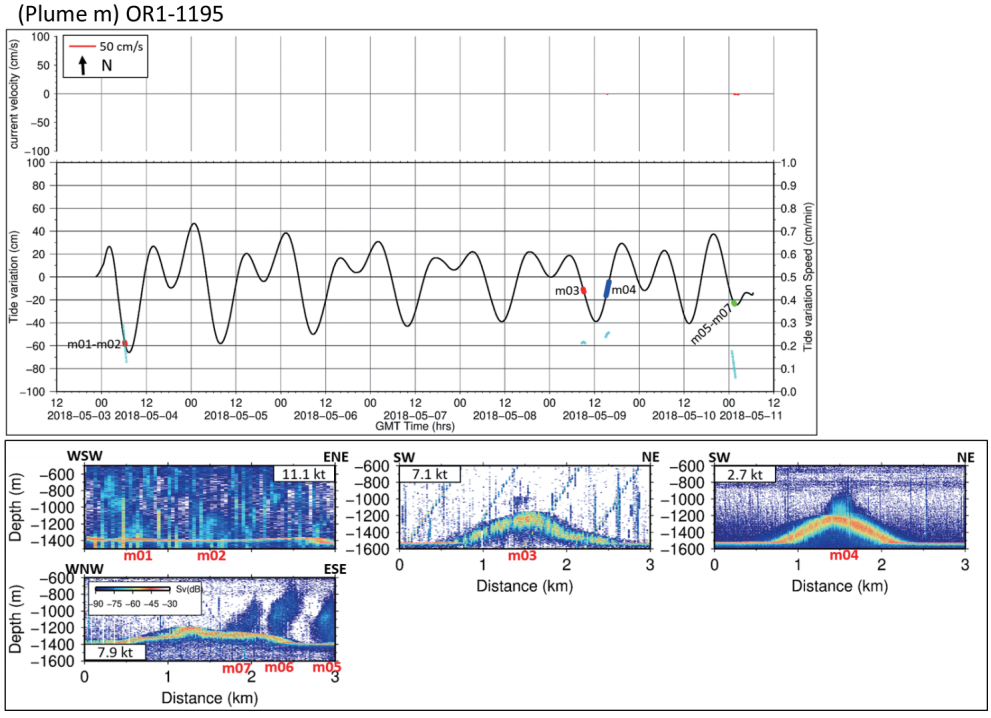

Fig. 16. EK60 images of the gas plumes of m-series. The relevant descriptions are shown in Fig. 4.

Table 1. List of gas plume tilt directions related to tidal changes in this study.

Cruise number	Plume number (figure number)	Ship-track direction									
		NE-SW		NW-SE		WNW-ESE		ENE-WSW		Others (NNW-SSE; N-S; NNE-SSW)	
OR1-1136	a (Fig. 4)	ebb	SW	low	SE						
		rising	NE								
OR1-1162	b (Fig. 5)	ebb	SW	ebb	NW						
		low	SW								
		rising	NW								
OR2-2055	c (Fig. 6)	rising	NE	rising	unclear					ebb	unclear
										low	S
										rising	NNW
										rising	N
										rising	NNE
OR2-2119	d (Fig. 7)	ebb	NE	low	NW						
		low	NE								
		rising	SW								
OR2-2120	e (Fig. 8)	low	NE								
		low	SW								
		rising	SW								
OR2-2159	f (Fig. 9)	ebb	SW			rising	ESE				
		rising	NE								
OR2-2160	g (Fig. 10)			low	unclear						
OR2-2163	h (Fig. 11)	ebb	SW	ebb	unclear			ebb	WSW		
		low	SW								
		rising	NE								
		high	NE								
OR2-2231	i (Fig. 12)	ebb	SW	ebb	unclear	ebb	WNW				
		rising	NE	rising	unclear						
OR2-2232	j (Fig. 13)	low	SW								
		rising	NE								
		high	NE								
		ebb	NE								
		rising	SW								
OR2-2289	k (Fig. 14)	ebb	SW			ebb	ESE				
		rising	NE								
		high	NE								
		ebb	NE								
		low	NE								
		rising	SW								
OR2-2290	l (Fig. 15)	low	SW								
		rising	NE								
		high	NE								
		ebb	NE								
OR1-1195	m (Fig. 16)	ebb	unclear			low	ESE	ebb	unclear		
		rising	unclear								

or at the lowest tides, the plume images incline to the southwest. As shown in d02 to d08 in Fig. 7, the plume images in the Keelung continental slope area incline to the southwest when the tide is rising. The plume images incline to the northeast when the tides are on the ebb. At the lowest tide, the plumes keep the same direction as on the ebb. However, in the areas around the Meinhua Canyon, there is no consistent tilt of the gas plumes (Fig. 13).

Furushima and Yamamoto (2015) have used ADCP to observe bottom currents in the Hatoma Knoll hydrothermal circulation area of the southern Okinawa Trough in April 2004 and May 2005. Their results showed that the bottom currents have a variation of 12-h semi-diurnal tidal cycle. During the rising tide, the water current flows northward; conversely, during the ebb tide, the water current flows southward. Their result is consistent with the results that we have observed the plume images in the central portion of the southwestern Okinawa Trough. Similarly, our deep-tow side-scan sonar images in Figs. 5 and 17 also indicate that the hydrothermal fluid from a single black chimney flows southward. Because the gas plumes keep the same direction at the rising tide to the highest tide and the same direction is on the ebb and at lowest tide, there could be a time lag effect of the tidal rise and fall effect on the flow of the water layer. It agrees with a stable flow of ~3 h during the transition of the rising and ebb (Furushima and Yamamoto 2015).

3.3 Near-Bottom Current Velocities Estimated from Gas Plume Images

As mentioned previously, the bottom currents as well as gas plume images can be affected by tidal variation. A real observation of the bottom current speeds will be implemented soon by ocean-bottom current meters by Academic Sinica. However, in the case of lacking real ADCP observations near seafloor, the tilted images of gas plumes from seabed could provide an alternative way to estimate near-seafloor current velocities. As illustrated in Fig. 18, a gas plume image is related to a bottom current velocity. We can measure each plume height h from the seafloor to the top of a plume, and the horizontal distance d. The rising time Δt of a gas bubble from the seafloor to the top of the plume could be calculated by h/Vp, where Vp is the upward velocity of the gas bubbles of the plume. Then, the near seafloor current velocity Vc can be calculated by $d/\Delta t$. In that case, the value Vp is a critical for calculating the current velocity Vc. Because the bottom-current velocity (Vc) is a linear function of upward velocity of the bubbles (Vp). The error estimation of the Vc is thus proportional to the error estimation of Vp.

Xu et al. (2013) have observed Vp of the hydrothermal plume of the Main Endeavour Field in the Juan de Fuca Ridge area by using the Cabled Observatory Vent Imaging Sonar (COVIS) instrument. They found the Vp of the hydrothermal plume is between 0.11 and 0.24 m s^{-1}. Using the temperature anomaly observed by CTD, Cen et al. (2017) have established a dynamic mode of the hydrothermal plume in the middle Okinawa Trough and obtained a Vp of 0.35 m s^{-1}. In the southern Okinawa Trough, Chi (2017) used ROV images of Wang (2016) and obtained a bubble rising velocity of 0.47 m s^{-1} in YK4-1 (Yonaguni Knoll IV-1) and 0.32 m s^{-1} in PFZ (Penglai Fault Zone) (Figs. 2 and 3).

Veloso et al. (2015) showed that clean or dirty bubbles have slightly different rising velocities. However, the bubbles in the middle or southern Okinawa Trough have faster rising velocities (Cen et al. 2017; Chi 2017). The reason could be ascribed to a very active backarc basin rifting and an active hydrothermal circulation in the Okinawa Trough. Here, we use the Vp value of 0.47 m s^{-1} from Chi (2017) to estimate the maximum near seafloor current velocities (Vc) in our study area. The results are shown in Table 2 and Figs. 4 to 16.

Belonged to 6 hydrothermal circulation zones, 11 plume images are used for further analysis (Table 1, Figs. 2, 4, 5, 11, and 13). Except for FDV-2 (Fire Dragon Volcano 2), the rest of the plumes are located near the rifting center of the Okinawa Trough (Figs. 2 and 3). Those plume images are detected along the survey tracks in the NE-SW orientation. The estimated current velocities are based on the rising speed of bubble at 0.47 m s^{-1} (Table 2). In the 6 hydrothermal circulation zones, the tides flow to the NE during the rising tide and the highest tide, and flow to the SW during the ebb tide and the lowest tide (Table 1). The gas plumes are situated in the water depths from 1150 to 1550 m (Table 2); in other words, the 7° beam width of EK60 indicates that the coverage of a single footprint is between 140 and 190 m in diameter. Hence, each of our estimated current velocities can be considered as an average of the near-seafloor current velocities from the bottom to the top of the gas plume. All the estimated near-seafloor current velocities are shown in Table 2.

Our estimated near-seafloor current velocities show the slowest velocity of 2.5 cm s^{-1} occurs in region YK4-1 and the fastest velocity of 156.9 cm s^{-1} occurs in region FDV-1 (Fire Dragon Volcano 1). As mentioned previously, tidal variations can affect gas plume directions and the directions of the currents. In order to understand the relationship between current velocities and the tidal variations, we calculated the slope change of the tides between 15 min before and after the plume recorded time (Table 2; Figs. 4 to 16). The results show that the slopes of the tides do not influence much the near-seafloor current velocities in region YK4-1. Nevertheless, the gas plumes i09 and i10 in submarine volcano region FDV-1 do display different tilt angles of plumes (Fig. 12), demonstrating the tidal variation influence. One possible reason is that the upward velocities of the bubbles (plumes) are different at two different times because the different emissions of the gases out of the seabed at different water pressures

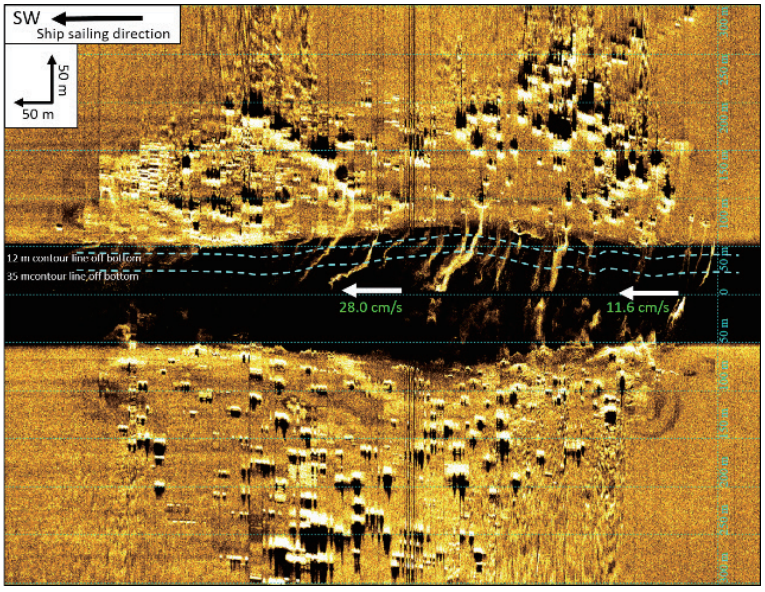

Fig. 17. Estimated near-seafloor current velocities in the deep-tow sidescan sonar image (Hsu 2017), collected simultaneously with plume image b21 in Fig. 5.

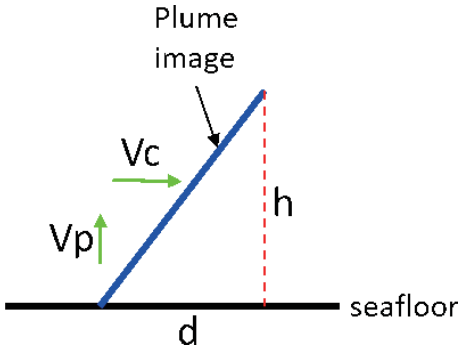

Fig. 18. Schematic relationship between current velocity Vc and upward gas bubbles (plume) float speed Vp. h is the height of the plume from the seabed; d is the horizontal distance of the plume tilt.

Table 2. Estimated near-seafloor current velocities (Vc) from 11 gas plumes.

Plume number (figure number)	distribution area	Water depth (m)	Plume height (m)	current velocity (cm s^{-1})	30-minute tidal slopes before and after the plume (cm min^{-1})
a08 (Fig. 4)	PFZ	-1447	628	34.0	0.579 - 0.359
b04 (Fig. 5)	PFZ	-1471	758	23.7	0.209 - 0.153
b10 (Fig. 5)	PFZ	-1503	573	28.6	0.032 - 0.064
h24 (Fig. 11)	PFZ	-1465	831	21.2	0.420 - 0.217
b19 (Fig. 5)	GLM	-1516	632	28.1	0.269 - 0.264
b21 (Fig. 5)	GLM	-1516	949	49.0	0.154 - 0.012
f05 (Fig. 9)	YK4-1	-1333	610	2.5	0.371 - 0.437
j09 (Fig. 13)	FDV-2	-1390	388	31.4	0.238 - 0.375
i14 (Fig. 12)	MHV	-1380	605	36.2	0.314 - 0.110
i19 (Fig. 12)	MHV	-1381	651	33.1	0.293 - 0.088
i09 (Fig. 12)	FDV-1	-1187	220	156.9	0.440 - 0.443

(depending on the tidal variation). The different inclusions of gases into the seawater can largely change the densities of the plumes and thus the buoyancies of the plumes.

As shown in Table 2, the near-seafloor currents show different velocities. However, it is remarkable that there is a large variation of estimated current velocities in the submarine volcanic area (in areas YK4-1, FDV-1, FDV-2, and MHV in Table 2). Tectonically, submarine volcanic areas contain more volcanic gases in the sediments, thus variable gas emissions and the upward velocities of the plumes appear in submarine volcanic areas. On the contrary, in the relatively "smooth" seafloor areas such as in regions PFZ and GLM (Geolin Mounds), the estimated current velocities are considerably consistent (Table 2). In fact, by using ADCP, Furushima and Yamamoto (2015) also observed variable current velocities at the same site; at 4 m above the seafloor, the current velocities can have a variation of 20 cm s^{-1}, and at 62 m above the seafloor the current velocities can have a variation of 50 cm s^{-1} (Furushima and Yamamoto 2015). Their observation is consistent with our values in plume b21 estimated from the deep-tow side-scan sonar (Fig. 4); the near-seafloor current velocity Vc has increased from 11.6 to 28.0 cm s^{-1}.

4. CONCLUSION

After analyzing the single-beam EK60 echo sounder data in the seawater and comparing the gas plume images with tides in the southernmost Okinawa Trough, we can draw the following conclusions.

(1) In total, 266 active gas plumes out of seabed are found. Most of the plumes are related to submarine volcanoes or hydrothermal circulation.

(2) In the middle of the southernmost Okinawa Trough, the lower boundary of thermocline generally appears around 600 m deep; therefore, most of the areas shallower than 600 m deep have a fairly thick suspension layer.

(3) The tilts of the gas plumes are changeable; they depend on the semi-diurnal tidal variation.

(4) In the middle of the southernmost Okinawa trough, the gas plumes incline to the northeast during the rising tide and highest tide, indicating that the near-seafloor current flows northeastward during that period. In contrast, the gas plumes incline to the southwest on the ebb tide and at low tide, indicating that the near-seafloor current flows southwestward during that period (Fig. 19).

(5) In the Keelung continental slope area, the gas plume images incline to the southwest at rising tide and highest tide, indicating a southwestward flow of the near-seafloor current. At ebb tide and low tide, the gas plume images incline to the northeast, indicating a northeastward flow of the near-seafloor current. This result is in opposite to the flows in the middle of the southernmost Okinawa Trough (Fig. 19).

(6) Our estimated velocities of the near-seafloor currents in the submarine volcanic area range between 2 and

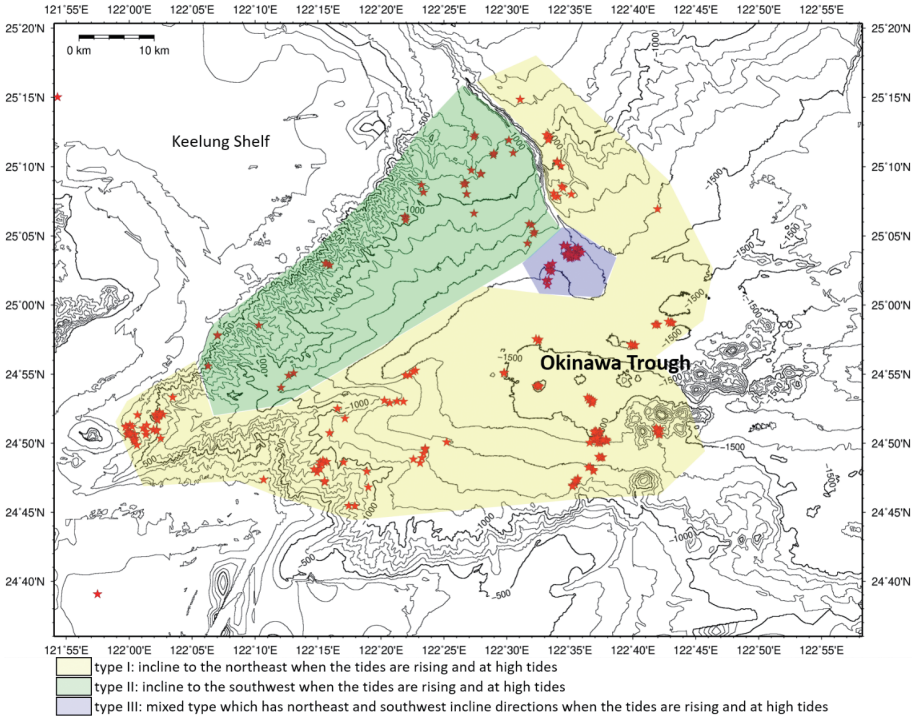

Fig. 19. The distribution of the gas plumes (red starts) and near-seafloor current patterns in the southernmost Okinawa Trough derived from acoustic echo sounders.

160 cm s^{-1}. However, in the relatively flat area, the near-seafloor currents are relatively stable with velocities between 20 and 50 cm s^{-1}. The rising bubbles (and plume) velocity used in the bottom current velocity estimation can be different and related to the quantity of the volcanic gas at each plume site, as gases in sediments are very compressible during a tidal variation.

(7) The near-seafloor bottom currents could be significantly estimated from EK plume images in the case of lacking real observations of bottom currents.

Acknowledgements This study was supported by the Ministry of Science and Technology (MOST) and the Central Geological Survey (CGS), Ministry of Economic Affairs, Taiwan. We appreciate the crew of R/V Ocean Researcher I and II for helping the collection of data.

REFERENCES

Aucan, J., M. A. Merrifield, D. S. Luther, and P. Flament, 2006: Tidal mixing events on the deep flanks of Kaena ridge, Hawaii. *J. Phys. Oceanogr.*, **36**, 1202-1219, doi: 10.1175/jpo2888.1. [Link]

Baker, E. T., C. R. German, and H. Elderfield, 1995: Hydrothermal plumes over spreading-center axes: Global distributions and geological inferences. In: Humphris, S. E., R. A. Zierenberg, L. S. Mullineaux, and R. E. Thomson (Eds.), Seafloor Hydrothermal Systems: Physical, Chemical, Biological, and Geological Interactions, Volume 91, American Geophysical Union, 47-71, doi: 10.1029/GM091p0047. [Link]

Berdeal, I. G., 2006: Hydrography and flow in the axial valley of the Endeavour segment: Implications for larval dispersal. Ph.D. Thesis, University of Washington, Washington, D. C.

Cen, X.-R., S.-X. Guo, Y.-Z. Lu, Q.-U. Ling, and S.-Q. Zhou, 2017: Numerical simulation of the dynamical processes of hydrothermal plumes in Okinawa trough. *Oceanologia et Limnologia Sinica*, **48**, 1435-1445, doi: 10.11693/hyhz20170500148. (in Chinese) [Link]

Chen, S.-C., S.-K. Hsu, C.-H. Tsai, C.-Y. Ku, Y.-C. Yeh, and Y. Wang, 2010: Gas seepage, pockmarks and mud volcanoes in the near shore of SW Taiwan. *Mar. Geophys. Res.*, **31**, 133-147, doi: 10.1007/s11001-010-9097-6. [Link]

Chi, W.-C., 2017: Geological Investigation of Mineral Resource Potential in the Offshore Northeastern Taiwan: Fluid migration modeling in the mineral resource potential area (2/4). Report of Central Geological Survey, 106-12-C, 45 pp. (in Chinese with English abstract)

Crone, T. J., W. S. D. Wilcock, and R. E. McDuff, 2010: Flow rate perturbations in a black smoker hydrothermal vent in response to a mid-ocean ridge earthquake swarm. *Geochem. Geophys. Geosyst.*, **11**, Q03012, doi: 10.1029/2009GC002926. [Link]

Fujioka, K. and K. Mitsuzawa, 2001: Tide-related variability of hydrothermal activity at the TAG hydrothermal mound, mid-Atlantic Ridge and the East Pacific Rise. *J. Geodetic Soc. Jap.*, **47**, 434-440, doi: 10.11366/sokuchi1954.47.434. [Link]

Fujioka, K., K. Kobayashi, K. Kato, M. Aoki, K. Mitsuzawa, M. Kinoshita, and A. Nishizawa, 1997: Tide-related variability of TAG hydrothermal activity observed by deep-sea monitoring system and OBSH. *Earth Planet. Sci. Lett.*, **153**, 239-250, doi: 10.1016/s0012-821x(97)00174-x. [Link]

Furushima, Y. and H. Yamamoto, 2015: Periodic Behavior of Deep Sea Current in the Hatoma Knoll Hydrothermal System. In: Ishibashi J., K. Okino, and M. Sunamura (Eds.), Subseafloor Biosphere Linked to Hydrothermal Systems, Springer, Tokyo, 625-637, doi: 10.1007/978-4-431-54865-2_50. [Link]

German, C. R., J. Briem, C. Chin, M. Danielsen, S. Holland, R. James, A. Jónsdóttir, E. Ludford, C. Moser, J. Ólafsson, M. R. Palmer, and M. D. Rudnicki, 1994: Hydrothermal activity on the Reykjanes Ridge: the Steinahóll vent-field at 63°06'N. *Earth Planet. Sci. Lett.*, **121**, 647-654, doi: 10.1016/0012-821x(94)90098-1. [Link]

Heeschen, K. U., A. M. Tréhu, R. W. Collier, E. Suess, and G. Rehder, 2003: Distribution and height of methane bubble plumes on the Cascadia Margin characterized by acoustic imaging. *Geophys. Res. Lett.*, **30**, doi: 10.1029/2003gl016974. [Link]

Hsu, S.-K., 2017: Geological Investigation of Mineral Resource Potential in the Offshore Northeastern Taiwan: High-resolution Sonar and Magnetic Surveys (2/4). Report of Central Geological Survey, 106-13, 237 pp. (in Chinese with English abstract)

Hsu, S.-K., J.-C. Sibuet, S. Monti, C.-T. Shyu, and C.-S. Liu, 1996: Transition between the Okinawa trough backarc extension and the Taiwan collision: New insights on the southernmost Ryukyu subduction zone. *Mar. Geophys. Res.*, **18**, 163-187, doi: 10.1007/bf00286076. [Link]

Hsu, S.-K., S.-S. Lin, S.-Y. Wang, C.-H. Tsai, W.-B. Doo, S.-C. Chen, J.-Y. Lin, Y.-C. Yeh, H.-F. Wang, and C.-W. Su, 2018: Seabed gas emissions and submarine landslides off SW Taiwan. *Terr. Atmos. Ocean. Sci.*, **29**, 7-15, doi: 10.3319/TAO.2016.10.04.01. [Link]

Kimura, M., 1985: Back-arc rifting in the Okinawa Trough. *Mar. Petrol. Geol.*, **2**, 222-240, doi: 10.1016/0264-8172(85)90012-1. [Link]

Kimura, M., I. Kaneoka, Y. Kato, S. Yamamoto, I. Kushiro, H. Tokuyama, H. Kinoshita, N. Isezaki, H. Masaki, A. Oshida, S. Uyeda, and T. W. C. Hilde, 1986: Report on DELP 1984 cruises in the middle Okinawa Trough Part V: Topography and geology of the central grabens and their vicinity. *Bulletin of the Earthquake Research Institute of Tokyo University*, **61**, 269-310.

Kimura, M., S. Uyeda, Y. Kato, T. Tanaka, M. Yamano, T. Gamo, H. Sakai, S. Kato, E. Izawa, and T. Oomori, 1988: Active hydrothermal mounds in the Okinawa Trough backarc basin, Japan. *Tectonophysics*, **145**, 319-324, doi: 10.1016/0040-1951(88)90203-x. [Link]

Lallemand, S. E., C.-S. Liu, and the ACT cruise scientific team, 1997: Swath bathymetry reveals active arc-continent collision near Taiwan. *Eos, Trans. AGU*, **78**, 173-175, doi: 10.1029/97eo00116. [Link]

Larson, B. I., E. J. Olson, and M. D. Lilley, 2007: In situ measurement of dissolved chloride in high temperature hydrothermal fluids. *Geochim. Cosmochim. Acta*, **71**, 2510-2523, doi: 10.1016/j.gca.2007.02.013. [Link]

Lee, C.-S., G.-G. Shor, L. D. Bibee, R.-S. Lu, and T. W. Hilde, 1980: Okinawa Trough: Origin of a back-arc basin. *Mar. Geol.*, **35**, 219-241, doi: 10.1016/0025-3227(80)90032-8. [Link]

Lee, Y.-L., 2005: The study of active submarine volcanoes and hydrothermal vents in the Southernmost Part of Okinawa Trough. Master Thesis, Institute of Applied Geophysics, National Taiwan Ocean University, Keelung, Taiwan, 44 pp. (in Chinese)

Letouzey, J. and M. Kimura, 1985: Okinawa Trough genesis: Structure and evolution of a backarc basin developed in a continent. *Mar. Petrol. Geol.*, **2**, 111-130, doi: 10.1016/0264-8172(85)90002-9. [Link]

Lin, J.-Y., J.-C. Sibuet, C.-S. Lee, S.-K. Hsu, and F. Klingelhoefer, 2007: Origin of the southern Okinawa Trough volcanism from detailed seismic tomography. *J. Geophys. Res.*, **112**, B08308, doi: 10.1029/2006JB004703. [Link]

Lin, J.-Y., J.-C. Sibuet, C.-S. Lee, S.-K. Hsu, F. Klingelhoefer, Y. Auffret, P. Pelleau, J. Crozon, and C.-H. Lin, 2009: Microseismicity and faulting in the southwestern Okinawa Trough. *Tectonophysics*, **466**, 268-280, doi: 10.1016/j.tecto.2007.11.030. [Link]

Massoth, G. J., H. B. Milburn, S. R. Hammond, D. A. Butterfield, R. E. McDuff, and J. E. Lupton, 1988: The geochemistry of submarine venting fluids at Axial Volcano, Juan de Fuca Ridge: New sampling methods and a VENTS Program rationale. In: De Luca, M. P. and I. Babb (Eds.), Global Venting, Midwater, and Benthic Ecological Processes, National Undersea Research Program Report 88-4, NOAA, Rockvile, MD, 29-59.

Matsumoto, K., T. Takanezawa, and M. Ooe, 2000: Ocean Tide Models Developed by Assimilating TOPEX/POSEIDON Altimeter Data into Hydrodynamical Model: A Global Model and a Regional Model around Japan. *J. Oceanogr.*, **56**, 567-581, doi: 10.1023/A:1011157212596. [Link]

Naudts, L., J. Greinert, Y. Artemov, P. Staelens, J. Poort, P. Van Rensbergen, and M. De Batist, 2006: Geological and morphological setting of 2778 methane seeps in the Dnepr paleo-delta, northwestern Black Sea. *Mar. Geol.*, **227**, 177-199, doi: 10.1016/j.margeo.2005.10.005. [Link]

Polikarpov, G. G., V. N. Egorov, A. I. Nezhdanonv, S. B. Gulin, Y. D. Kulev, and M. B. Gulin, 1989: Methane gas seeps in the Black Sea: A new object of molismology. In: Polikarpov, G. G. (Ed.), Molismology of the Black Sea, Kiev, Nauka, 10-20.

Seno, T., S. Stein, and A. E. Gripp, 1993: A model for the motion of the Philippine Sea Plate consistent with NUVEL-1 and geological data. *J. Geophys. Res.*, **98**, 17941-17948, doi: 10.1029/93JB00782. [Link]

Shyu, C.-T. and C.-S. Liu, 2001: Heat Flow of the Southwestern End of the Okinawa Trough. *Terr. Atmos. Ocean. Sci.*, **12**, 305-317, doi: 10.3319/TAO.2001.12.S.305(ODP). [Link]

Sibuet, J.-C., J. Letouzey, F. Barbier, J. Charvet, J.-P. Foucher, T. W. C. Hilde, M. Kimura, L.-Y. Chiao, B. Marsset, C. Muller, and J.-F. Stéphan, 1987: Back arc extension in the Okinawa Trough. *J. Geophys. Res.*, **92**, 14041-14063, doi: 10.1029/JB092iB13p14041. [Link]

Sibuet, J.-C., B. Deffontaines, S.-K. Hsu, N. Thareau, J. P. Le Formal, C.-S. Liu, and ACT party, 1998: Okinawa Trough backarc basin: Early tectonic and magmatic evolution. *J. Geophys. Res.*, **103**, 30245-30267, doi: 10.1029/98jb01823. [Link]

Tsai, C.-H., 1999: Submarine Volcanoes and Hydrothermal Circulation in the Southernmost Part of Okinawa Trough: An Initial Study. Master Thesis, Institute of Applied Geophysics, National Taiwan Ocean University, Keelung, Taiwan, 82 pp. (in Chinese)

Urban, P., K. Köser, and J. Greinert, 2017: Processing of multibeam water column image data for automated bubble/seep detection and repeated mapping. *Limnol. Oceanogr.*, **15**, 1-21, doi: 10.1002/lom3.10138. [Link]

Uyeda, S., 1977: Some basic problems in the trench-arc-back arc system. In: Talwani, M. and W. C. Pitman (Eds.), Island Arcs, Deep Sea Trenches and Back-Arc Basins, Volume 1, American Geophysical Union, Washington, DC, 1-14, doi: 10.1029/ME001p0001. [Link]

Veirs, S. R., R. E. McDuff, and F. R. Stahr, 2006: Magnitude and variance of near-bottom horizontal heat flux at the Main Endeavour hydrothermal vent field. *Geochem. Geophys. Geosyst.*, **7**, doi: 10.1029/2005gc000952. [Link]

Veloso, M., J. Greinert, J. Mienert, and M. De Batist, 2015: A new methodology for quantifying bubble flow rates in deep water using splitbeam echosounders: Examples from the Arctic offshore NW-Svalbard. *Limnol. Oceanogr.*, **13**, 267-287, doi: 10.1002/lom3.10024. [Link]

Wang, C.-C., 2016: Geological Investigation of Mineral Resource Potential in the Offshore Northeastern Taiwan: Video Surveys and Sampling of Seafloor Mineral Deposits (1/4). Report of Central Geological Survey, 105-14-B, 70 pp. (in Chinese with English abstract)

Xu, G., D. R. Jackson, K. G. Bemis, and P. A. Rona, 2013: Observations of the volume flux of a seafloor hydrothermal plume using an acoustic imaging sonar. *Geochem. Geophys. Geosyst.*, **14**, 2369-2382, doi: 10.1002/ggge.20177. [Link]

Yu, S.-B., H.-Y. Chen, and L.-C. Kuo, 1997: Velocity field of GPS stations in the Taiwan area. *Tectonophysics*, **274**, 41-59, doi: 10.1016/s0040-1951(96)00297-1. [Link]

APPENDIX A

Table A1. The detailed information of 266 plume images in this study (remark A means complete plume image; remark B means incomplete plume image).

No.	longitude (degree:minute)	latitude (degree:minute)	water depth (m)	observation date (dd/mm/yyyy)	observation time (hh:mm:ss)	ship speed (kts)	plume height (m)	tidal type	remark
a01	121:47.43576	25:12.56184	-113	07/05/2016	03:26:32				B
a02	121:47.63472	25:12.55806	-107	07/05/2016	03:27:33				B
a03	121:47.65872	25:12.55668	-107	07/05/2016	03:27:41	8.6	47	ebb	A
a04	121:50.74851	25:12.56010	-124	07/05/2016	09:39:17				B
a05	121:47.58168	25:10.59646	-54	07/05/2016	09:40:31				B
a06	121:50.98935	25:10.59184	-88	07/05/2016	03:27:40				B
a07	122:41.86062	24:58.59666	-1485	07/05/2016	15:32:30	2.5	340	ebb	A
a08	122:37.91028	24:50.23554	-1447	08/05/2016	04:02:26	2.1	628	ebb	A
a09	122:37.51998	24:48.97314	-1335	08/05/2016	12:20:15	2.4	553	high tide to ebb	A
a10	122:37.29696	24:50.06250	-1447	08/05/2016	13:30:13	10.7	460	ebb	A
a11	122:43.00716	24:58.69914	-1494	08/05/2016	14:24:51				B
a12	122:43.05498	24:58.76298	-1478	08/05/2016	15:08:54	2.3	326	ebb	A
a13	122:36.89502	24:47.97881	-1267	08/05/2016	21:32:34	1.9	442	rising	A
a14	122:37.01140	24:50.22617	-1466	09/05/2016	15:17:59	11.7	800	ebb	A
a15	122:37.13220	24:50.37137	-1479	09/05/2016	15:18:54	11.7	142	ebb	A
a16	122:37.28952	24:50.07708	-1448	10/05/2016	06:05:48	1.4	605	ebb	A
a17	122:36.87420	24:50.27052	-1474	10/05/2016	08:17:10	11.8	432	rising	A
a18	122:37.15296	24:50.57274	-1486	10/05/2016	08:19:03	11.8	690	rising	A
a19	122:36.95040	24:50.24094	-1470	10/05/2016	13:07:56	10	670	rising	A
a20	122:37.12314	24:50.45832	-1482	10/05/2016	13:09:36	10	826	rising	A
a21	122:41.86537	24:50.80725	-1377	12/05/2016	08:59:57	2.1	250	low tide	A
a22	122:42.04920	24:50.61720	-1396	12/05/2016	09:07:40	2.1	216	low tide	A
a23	122:15.55134	24:47.17074	-743	12/05/2016	19:45:07	8.9	132	ebb	A
a24	121:57.50070	24:39.05388	-126	13/05/2016	05:55:30				B
a25	122:22.27182	24:54.94032	-1309	13/05/2016	20:08:50				B
a26	122:34.71846	25:03.57126	-1355	14/05/2016	21:04:10	11.7	873	ebb	A
a27	122:34.90614	25:04.02223	-1225	14/05/2016	23:13:05	2.1	590	ebb	A
a28	122:34.68302	25:03.68023	-1315	14/05/2016	23:23:10	2.1	200	ebb	A
a29	122:33.24162	25:1.433700	-1409	15/05/2016	00:25:28				B
a30	121:49.97292	25:13.04082	-123	15/05/2016	05:53:49				B
b01	122:36.53412	24:53.182080	-1516	18/04/2017	17:30:37	4.7	719	ebb	A
b02	122:37.33144	24:50.828171	-1486	19/04/2017	08:09:58	1.9	763	ebb	A
b03	122:37.19129	24:50.546268	-1486	19/04/2017	08:19:39	1.9	784	ebb	A
b04	122:37.06395	24:50.296641	-1471	19/04/2017	08:27:47	1.9	758	ebb	A
b05	122:35.62902	24:47.426212	-1252	19/04/2017	10:00:08	2.4	476	low tide	A
b06	122:35.57349	24:47.320465	-1234	19/04/2017	10:03:34	2.4	434	low tide	A
b07	122:35.41258	24:47.026960	-1211	19/04/2017	10:13:07	2.4	481	low tide	A
b08	122:36.69654	24:52.912200	-1515	19/04/2017	12:10:16	2.4	768	rising	A
b09	122:40.13232	24:57.080820	-1401	19/04/2017	15:55:59	2	652	rising	A
b10	122:37.03319	24:50.883776	-1503	19/04/2017	19:21:23	2.2	573	ebb	A
b11	122:35.21622	24:46.935120	-1209	19/04/2017	21:25:42				B
b12	122:35.20493	24:46.871271	-1209	19/04/2017	22:24:25				B

Table A1. (Continued)

No.	longitude (degree:minute)	latitude (degree:minute)	water depth (m)	observation date (dd/mm/yyyy)	observation time (hh:mm:ss)	ship speed (kts)	plume height (m)	tidal type	remark
b13	122:35.42186	24:47.298994	-1224	19/04/2017	22:26:59				B
b14	122:36.86601	24:50.239885	-1472	19/04/2017	22:44:25	11.3	769	low tide	A
b15	122:37.03230	24:50.573263	-1495	19/04/2017	22:46:23	11.3	719	low tide	A
b16	122:37.13851	24:50.792554	-1491	19/04/2017	22:47:39	11.3	752	low tide	A
b17	122:39.84594	24:57.167280	-1405	20/04/2017	02:17:38				B
b18	122:39.96714	24:57.082560	-1392	20/04/2017	09:35:52	11.4	752	ebb	A
b19	122:36.78618	24:53.001780	-1516	21/04/2017	09:57:05	1.7	632	ebb	A
b20	122:36.68766	24:53.148600	-1514	22/04/2017	16:35:10	5.2	911	rising	A
b21	122:36.54606	24:53.174400	-1516	23/04/2017	02:01:34	2.5	949	ebb	A
b22	122:36.41460	24:53.297880	-1516	25/04/2017	22:45:43				B
b23	121:54.31500	25:15.025560	-139	26/04/2017	08:46:02				B
c01	122:7.04100	24:57.77640	-399	17/09/2014	13:36:32	6.8	78	rising	A
c02	122:7.02564	24:57.83544	-384	17/09/2014	13:37:02	6.8	90	rising	A
c03	122:6.27378	24:55.58400	-531	17/09/2014	17:00:40	5.6	118	rising	A
c04	122:3.46080	24:53.31174	-612	18/09/2014	00:03:17				B
c05	122:2.68920	24:52.07862	-583	18/09/2014	02:37:20	7.2	292	rising	A
c06	122:2.42334	24:52.24362	-482	18/09/2014	05:01:27	5.2	104	rising	A
c07	122:2.42065	24:52.07774	-506	18/09/2014	05:02:55	5.2	180	rising	A
c08	122:2.41783	24:52.01381	-516	18/09/2014	05:03:29	5.2	55	rising	A
c09	122:2.19052	24:50.96919	-533	18/09/2014	05:13:15	5.2	87	rising	A
c10	122:1.93262	24:50.95265	-476	18/09/2014	05:20:21	7.4	98	rising	A
c11	122:1.95074	24:50.99587	-476	18/09/2014	05:20:57	7.4	104	rising	A
c12	122:2.09602	24:51.97487	-472	18/09/2014	05:30:59	7.4	120	rising	A
c13	122:2.09150	24:52.09888	-461	18/09/2014	05:32:01	7.4	100	rising	A
c14	122:1.33779	24:50.62721	-386	18/09/2014	08:25:37				B
c15	122:1.36107	24:50.83574	-424	18/09/2014	08:27:23				B
c16	122:1.38907	24:51.29688	-457	18/09/2014	08:31:13				B
c17	122:1.11996	24:51.08898	-430	18/09/2014	11:06:37	6.9	262	ebb	A
c18	122:0.67374	24:52.02895	-337	18/09/2014	13:58:12				B
c19	122:0.46198	24:50.61269	-253	18/09/2014	14:10:14	5.6	142	low tide	A
c20	122:0.43200	24:50.33287	-291	18/09/2014	14:12:34	5.6	128	low tide	A
c21	122:0.42266	24:50.25845	-286	18/09/2014	14:13:12	5.6	170	low tide	A
c22	122:0.40357	24:50.13377	-265	18/09/2014	14:14:16	5.6	166	low tide	A
c23	122:0.24690	24:51.20742	-378	18/09/2014	14:31:58				B
c24	122:0.07374	24:51.34416	-363	18/09/2014	16:52:02	7.1	66	rising	A
c25	121:59.9886	24:50.81712	-248	18/09/2014	16:56:36	7.1	174	rising	A
c26	121:59.9654	24:50.69910	-242	18/09/2014	16:57:38	7.1	201	rising	A
c27	121:59.9569	24:50.66605	-238	18/09/2014	16:57:56	7.1	150	rising	A
c28	121:59.9012	24:50.59674	-228	18/09/2014	16:59:00	7.1	124	rising	A
c29	121:59.8626	24:50.59939	-226	18/09/2014	16:59:32	7.1	213	rising	A
c30	121:59.7106	24:51.16032	-291	18/09/2014	17:06:36				B
c31	121:59.7526	24:51.22082	-295	19/09/2014	03:13:46	7.8	63	rising	A
c32	121:59.9946	24:50.82802	-251	19/09/2014	03:17:05	7.8	63	rising	A
c33	122:0.03654	24:50.75773	-250	19/09/2014	03:17:41	7.8	196	rising	A
c34	122:0.09400	24:50.68038	-257	19/09/2014	03:18:23	7.8	79	rising	A
c35	122:0.34722	24:50.29332	-252	19/09/2014	03:21:45	7.8	126	rising	A
c36	122:0.44634	24:50.14902	-278	19/09/2014	03:23:01	7.8	150	rising	A
c37	122:0.62826	24:49.85712	-307	19/09/2014	03:25:29				B
c38	122:2.49906	24:50.35044	-572	19/09/2014	06:03:37				B
c39	122:2.20578	24:50.89254	-535	19/09/2014	06:08:35				B

Table A1. (Continued)

No.	longitude (degree:minute)	latitude (degree:minute)	water depth (m)	observation date (dd/mm/yyyy)	observation time (hh:mm:ss)	ship speed (kts)	plume height (m)	tidal type	remark
c40	122:2.23211	24:51.66115	-517	19/09/2014	06:15:47	7.4	123	rising	A
c41	122:2.26786	24:51.72484	-522	19/09/2014	06:16:21	7.4	140	rising	A
c42	122:2.40032	24:51.96696	-527	19/09/2014	06:18:31	7.4	83	rising	A
c43	122:2.46990	24:52.09873	-528	19/09/2014	06:19:41	7.4	143	rising	A
d01	122:27.45384	25:12.27260	-799	16/09/2015	16:20:47	4.6	234	ebb	A
d02	122:27.17598	25:09.72342	-808	17/09/2015	07:37:10	5.8	76	rising	A
d03	122:28.92708	25:10.83370	-902	17/09/2015	07:57:52	5	246	rising	A
d04	122:27.96828	25:09.46422	-938	17/09/2015	08:39:01	6.1	291	rising	A
d05	122:26.72466	25:08.77878	-930	17/09/2015	08:52:04	5.4	258	rising	A
d06	122:21.95070	25:06.12684	-932	17/09/2015	09:41:22				B
d07	122:26.79012	25:08.02368	-968	17/09/2015	15:11:56	6.8	185	ebb	A
d08	122:10.30632	24:58.53470	-610	17/09/2015	18:50:23	6.2	158	low tide	A
e01	122:13.07700	24:55.06990	-1103	21/09/2015	09:41:16	6.2	417	rising	A
e02	122:12.67112	24:54.90132	-1072	21/09/2015	09:45:16	6.2	368	rising	A
e03	122:12.07674	24:54.02088	-1102	21/09/2015	10:00:16	6.4	228	rising	A
e04	122:35.93888	25:03.80614	-1363	21/09/2015	22:23:36				B
e05	122:35.50185	25:03.60770	-1388	21/09/2015	22:28:04	5.4	775	low tide	A
e06	122:35.00175	25:03.36039	-1386	21/09/2015	22:33:20	5.4	735	low tide	A
e07	122:33.45720	25:02.60808	-1400	21/09/2015	22:48:40	6.3	809	low tide	A
e08	122:34.48506	25:04.29324	-1325	21/09/2015	23:42:28	6	328	low tide	A
e09	122:34.35660	25:08.58780	-1177	22/09/2015	05:52:24				B
e10	122:33.28500	25:12.03930	-857	22/09/2015	11:29:56	5.9	293	low tide	A
e11	122:33.24990	25:12.27204	-877	22/09/2015	12:00:56	6.3	268	low tide	A
e12	122:30.50538	25:10.99218	-916	22/09/2015	13:53:12	6.4	466	rising	A
e13	122:30.16170	25:11.91012	-881	22/09/2015	15:27:45	5.1	184	rising	A
e14	122:31.04928	25:14.85156	-790	22/09/2015	16:24:21				B
f01	122:33.37920	25:02.73180	-1825	19/04/2016	07:32:58	6.4	997	rising	A
f02	122:42.17064	24:50.61978	-1397	21/04/2016	14:18:39	4.8	571	ebb	A
f03	122:42.06510	24:50.77866	-1348	21/04/2016	14:55:39	5.2	668	ebb	A
f04	122:42.18024	24:51.01878	-1219	21/04/2016	14:58:31	5.2	354	ebb	A
f05	122:41.97792	24:50.96232	-1333	21/04/2016	18:50:31	5.2	610	rising	A
f06	122:41.86212	24:51.09972	-1302	21/04/2016	19:17:51	5.3	608	rising	A
g01	122:33.62808	25:02.99238	-1382.00	26/04/2016	06:31:35.6	8.3	212	low tide	A
h01	122:42.04206	24:50.83140	-1375	05/05/2016	13:18:11	12	647	ebb	A
h02	122:43.16988	24:58.69440	-1498	06/05/2016	17:05:40	6.2	660	rising	A
h03	122:42.97428	24:58.69782	-1500	06/05/2016	21:01:40	5.8	328	rising	A
h04	122:42.82872	24:58.79136	-1481	05/06/2016	21:37:07				B
h05	122:41.98362	24:58.58502	-1491	07/05/2016	06:49:28	5.5	460	rising	A
h06	122:37.59948	24:48.97866	-1338	07/05/2016	08:34:36	5.9	299	rising	A
h07	122:37.41108	24:48.92952	-1334	07/05/2016	08:55:04	5.9	140	rising	A
h08	122:37.95426	24:50.12514	-1447	07/05/2016	09:08:12				B
h09	122:41.77320	24:58.54824	-1488	07/05/2016	10:40:16	5.9	415	rising	A
h10	122:37.84356	24:50.26794	-1449	07/05/2016	12:56:12				B
h11	122:37.29138	24:49.02384	-1340	07/05/2016	13:10:28				B
h12	122:36.85944	24:48.06066	-1274	07/05/2016	13:21:20	5.2	541	ebb	A
h13	122:37.64544	24:50.20494	-1457	07/05/2016	13:47:40				B
h14	122:37.46962	24:50.16793	-1461	07/05/2016	17:20:04	5.5	452	rising	A
h15	122:37.41507	24:50.05328	-1442	07/05/2016	17:21:20	5.5	400	rising	A
h16	122:37.38773	24:49.98682	-1428	07/05/2016	17:22:04	5.5	352	rising	A
h17	122:36.62244	24:48.28260	-1292	07/05/2016	17:41:00	5.9	203	rising	A

Table A1. (Continued)

No.	longitude (degree:minute)	latitude (degree:minute)	water depth (m)	observation date (dd/mm/yyyy)	observation time (hh:mm:ss)	ship speed (kts)	plume height (m)	tidal type	remark
h18	122:36.46548	24:48.24186	-1287	07/05/2016	17:49:36	5.6	545	rising	A
h19	122:37.22454	24:50.02332	-1440	07/05/2016	18:08:48	5.4	776		A
h20	122:40.20090	24:57.11874	-1405	07/05/2016	20:32:12	5.8	384	rising	A
h21	122:37.43281	24:50.83457	-1490	07/05/2016	21:40:36	5.8	843	rising	A
h22	122:37.34504	24:50.63361	-1488	07/05/2016	21:42:56	5.8	805	rising	A
h23	122:37.25904	24:50.44596	-1482	07/05/2016	21:45:08	5.8	833	rising	A
h24	122:37.16016	24:50.23662	-1465	07/05/2016	21:47:40	5.8	831	rising	A
h25	122:37.01454	24:50.23770	-1466	07/05/2016	22:44:24	5.8	739	high tide	A
h26	122:37.17618	24:50.62746	-1487	07/05/2016	22:48:52	5.8	771	high tide	A
h27	122:39.99144	24:57.05250	-1384	08/05/2016	00:00:00				B
h28	122:39.83514	24:57.15108	-1402	08/05/2016	01:12:08				B
h29	122:37.11696	24:50.82839	-1495	08/05/2016	02:25:04	6.2	791	ebb	A
h30	122:36.87783	24:50.32349	-1481	08/05/2016	02:31:52	6.2	715	ebb	A
h31	122:36.58740	24:50.03958	-1417	08/05/2016	03:30:12	5.8	291	ebb	A
h32	122:36.92208	24:50.80584	-1506	08/05/2016	03:38:32	5.8	548	ebb	A
h33	122:36.76464	24:52.86552	-1515	08/05/2016	17:26:20	6.1	537	low tide	A
h34	122:36.72912	24:53.17368	-1516	08/05/2016	20:02:08	5.6	934	rising	A
h35	122:36.53694	24:53.13180	-1515	08/05/2016	21:32:04	5.6	685	rising	A
h36	122:15.91903	25:02.87999	-776	09/05/2016	02:30:56				B
h37	122:15.72340	25:02.95878	-715	09/05/2016	02:32:12				B
h38	122:15.58939	25:03.01194	-659	09/05/2016	02:33:04				B
i01	122:36.56627	24:53.23438	-1513	07/04/2017	07:35:02	4.9	922	rising	A
i02	122:36.84848	24:53.06042	-1514	07/04/2017	07:37:47	4.9	771	rising	A
i03	122:37.50606	24:50.19276	-1460	07/04/2017	08:41:11	6.9	726	ebb	A
i04	122:37.19286	24:50.37870	-1477	07/04/2017	08:44:24	6.9	855	ebb	A
i05	122:41.97390	25:06.93762	-1385	07/04/2017	13:52:12	6.0	971	ebb	A
i09	122:32.54004	24:54.13110	-1187	10/04/2017	13:25:25	6.5	220	ebb	A
i10	122:32.31738	24:54.14604	-1303	10/04/2017	16:13:46	6.4	724	low tide	A
i11	122:35.61846	25:03.45132	-1377	11/04/2017	01:58:19	5.9	602	ebb	A
i12	122:35.76450	25:03.80796	-1373	11/04/2017	02:01:50	5.9	624	ebb	A
i13	122:35.79810	25:03.90120	-1372	11/04/2017	02:02:41	5.9	355	ebb	A
i14	122:35.66838	25:04.15384	-1380	11/04/2017	03:59:27	5.7	605	ebb	A
i15	122:35.61835	25:04.02019	-1373	11/04/2017	04:00:48	5.7	209	ebb	A
i16	122:35.55865	25:03.87180	-1374	11/04/2017	04:02:18	5.7	301	ebb	A
i17	122:35.46471	25:03.64079	-1388	11/04/2017	04:04:43	5.7	655	ebb	A
i18	122:35.12118	25:03.39624	-1387	11/04/2017	10:17:06	5.4	155	rising	A
i19	122:35.25898	25:03.72546	-1381	11/04/2017	10:20:42	5.4	651	rising	A
i20	122:35.40202	25:04.10702	-1387	11/04/2017	10:25:07	5.4	522	rising	A
i21	122:35.06496	25:03.81289	-1326	11/04/2017	12:42:00	6.6	314	ebb	A
i22	122:34.94747	25:03.51430	-1369	11/04/2017	12:45:21	6.6	761	ebb	A
i23	122:32.53968	24:57.50520	-1487	11/04/2017	13:52:30	5.7	530	ebb	A
i24	122:32.49528	24:57.38904	-1489	11/04/2017	13:53:42	5.7	794	ebb	A
i25	122:32.32482	24:57.54444	-1489	11/04/2017	18:32:37	6.2	952	rising	A
i26	122:34.72758	25:03.55866	-1362	11/04/2017	19:54:49	4.9	948	rising	A
i27	122:34.79928	25:04.29942	-1329	11/04/2017	22:30:33	5.2	726	rising	A
i28	122:22.75344	24:55.27152	-1314	12/04/2017	04:22:16	8.9	356	ebb	A
j01	122:34.54716	25:04.27806	-1323	13/04/2017	10:17:32	8.9	250	rising	A
j02	122:33.57534	25:02.42076	-1401	13/04/2017	12:42:40	5.2	360	high tide	A
j03	122:33.32256	25:01.80990	-1411	13/04/2017	12:49:40	5.2	350	high tide	A
j04	122:33.08934	25:01.77259	-1410	13/04/2017	18:38:11	6.4	285	rising	A

Table A1. (Continued)

No.	longitude (degree:minute)	latitude (degree:minute)	water depth (m)	observation date (dd/mm/yyyy)	observation time (hh:mm:ss)	ship speed (kts)	plume height (m)	tidal type	remark
j05	122:33.36570	25:02.45893	-1404	13/04/2017	18:56:19	6.8	990	rising	A
j06	122:33.39529	25:02.53489	-1402	13/04/2017	18:58:51	6.8	706	rising	A
j07	122:33.28068	25:02.83188	-1396	13/04/2017	21:35:35				B
j08	122:35.12502	25:07.99194	-1207	14/04/2017	04:59:39	5.4	320	ebb	A
j09	122:29.79868	24:55.11381	-1390	14/04/2017	08:02:27	6.3	388	rising	A
j10	122:34.46501	25:08.46681	-1165	15/04/2017	15:30:37				B
j11	122:34.01034	25:07.85514	-1180	15/04/2017	16:09:25	5.8	611	ebb	A
j12	122:33.80892	25:07.82325	-1150	16/04/2017	00:11:49				B
j13	122:33.71219	25:08.08471	-1110	16/04/2017	00:54:53	5.5	168	high tide	A
j14	122:32.18146	25:05.27541	-1298	16/04/2017	10:39:25	6.4	818	rising	A
j15	122:32.13055	25:05.14374	-1307	16/04/2017	10:40:49	6.4	575	rising	A
j16	122:31.63586	25:04.45576	-1273	16/04/2017	18:03:09	5.8	475	ebb	A
j17	122:31.97088	25:05.79804	-1223	16/04/2017	19:47:49	6.5	502	low tide	A
j18	122:31.76810	25:05.87408	-1174	17/04/2017	01:17:09				B
j19	122:34.00046	25:10.38862	-939	17/04/2017	05:02:54				B
j20	122:33.96796	25:10.30323	-969	17/04/2017	05:03:54				B
j21	122:34.29048	25:10.03050	-992	17/04/2017	05:30:46	5.8	286	ebb	A
k01	121:51.08244	25:10.64736	104	14/03/2018	03:57:19	5.1	97	ebb	A
k02	122:10.69314	24:47.34618	223	14/03/2018	09:16:01	4.9	88	high tide to ebb	A
k03	122:14.68548	24:48.11568	795	14/03/2018	11:33:54				B
k04	122:14.92976	24:47.87954	700	14/03/2018	14:10:38	6.3	104	ebb	A
k0S	122:15.10925	24:48.39673	794	14/03/2018	14:16:08	6.3	157	ebb	A
k06	122:15.18323	24:48.62531	855	14/03/2018	14:18:32	6.3	114	ebb	A
k07	122:15.92268	24:so.72676	1462	14/03/2018	14:40:41				B
k08	122:16.54356	24:52.50714	398	14/03/2018	15:00:05	6	224	low tide	A
k09	122:15.38660	24:48.74790	905	14/03/2018	19:45:35				B
k10	122:15.30876	24:48.48746	834	14/03/2018	19:48:53				B
k11	122:15.16673	24:48.12952	719	14/03/2018	19:53:36	4.8	104	rising	A
k12	122:15.52032	24:48.62100	923	14/03/2018	22:24:18	5	205	high tide to ebb	A
k13	122:21.86868	25:06.35471	888	15/03/2018	01:51:09	4.6	235	ebb	A
k14	122:21.89781	25:06.41817	853	15/03/2018	01:51:54	4.6	198	ebb	A
k1S	122:22.00404	25:06.28512	908	15/03/2018	02:01:30	4.5	267	ebb	A
k16	122:15.70200	24:48.64770	903	15/03/2018	05:25:52	6.2	215	rising	A
k17	122:23.21718	25:08.68632	788	15/03/2018	13:18:53	5.4	258	ebb	A
k18	122:17.14644	24:51.78942	1151	15/03/2018	16:27:04				B
k19	122:15.51900	24:47.24934	711	15/03/2018	17:18:58	5.2	86	rising	A
k20	122:23.39412	25:08.12904	911	15/03/2018	23:14:10	5.9	253	high tide to ebb	A
k21	122:17.04258	24:48.60810	976	16/03/2018	07:44:07	4.6	271	rising	A
k22	122:17.45004	24:45.46896	760	19/03/2018	15:17:16	5.9	160	ebb	A
k23	122:20.27982	24:53.09664	1116	18/03/2018	16:44:37	5.8	520	ebb	A
k24	122:27.37884	25:12.14142	770	18/03/2018	20:19:49				B
k25	122:26.61870	25:08.81052	932	18/03/2018	21:01:37				B
k26	122:26.58204	25:08.70516	938	18/03/2018	21:02:46				B
k27	122:20.69670	24:52.91262	1188	19/03/2018	00:06:06				B
k28	122:18.86118	24:47.94852	810	19/03/2018	01:04:27				B
k29	122:17.94060	24:45.43818	804	19/03/2018	01:32:35	5.4	154	ebb	A
k30	122:21.27000	24:53.03172	1204	19/03/2018	03:56:51				B
k31	122:21.96660	24:54.90984	1364	19/03/2018	04:18:38				B
k32	122:26.82264	25:08.01192	977	19/03/2018	06:52:31	5.3	460	rising	A
k33	122:27.90834	25:09.49254	943	19/03/2018	08:15:58	6.4	260	rising	A

Table A1. (Continued)

No.	longitude (degree:minute)	latitude (degree:minute)	water depth (m)	observation date (dd/mm/yyyy)	observation time (hh:mm:ss)	ship speed (kts)	plume height (m)	tidal type	remark
l01	122:22.58058	24:55.19514	1316	22/03/2018	10:57:08				B
l02	122:27.38316	25:66.62448	1055	22/03/2018	13:29:49				B
l03	122:28.93146	25:10.84356	912	22/03/2018	14:17:41	5.4	156	high tide	A
l04	122:28.96914	25:10.95924	907	22/03/2018	14:18:55	5.4	237	high tide	A
l05	122:21.79782	24:53.01264	1233	22/03/2018	22:08:47	5.4	535	rising	A
l06	122:22.58346	24:48.83064	1113	23/03/2018	10:56:08	6.1	195	rising	A
l07	122:23.11652	24:48.55148	1178	23/03/2018	12:52:20				B
l08	122:23.25352	24:48.92977	1163	23/03/2018	12:56:32				B
l09	122:23.38523	24:49.24968	1166	23/03/2018	13:00:11	5.5	630	rising	A
l10	122:23.48298	24:49.54314	1204	23/03/2018	13:03:26				B
l11	122:23.51394	24:49.62876	1263	23/03/2018	13:04:23	5.5	265	rising	A
l12	122:33.13134	25:12.28986	891	24/03/2018	05:11:10				B
l13	122:33.37064	25:12.12494	865	24/03/2018	05:20:10	5.6	135	ebb	A
l14	122:33.30584	25:11.92467	896	24/03/2018	05:22:28				B
l15	122:25.22646	24:50.06544	1310	24/03/2018	09:25:47	5.7	465	low tide	A
l16	122:18.99276	24:46.81308	872	24/03/2018	11:38:26	6	136	rising	A
l17	122:29.75856	24:55.05750	1284	25/03/2018	00:23:56	4.2	780	rising	A
m01	122:34.96194	25:03.48648	-1366	04/05/2018	06:13:19	11.1	855	ebb	A
m02	122:35.47140	25:03.60918	-1380	04/05/2018	06:16:07	11.1	879	ebb	A
m03	122:32.58720	24:54.07938	-1133	09/05/2018	09:03:58	7.1	218	ebb	A
m04	122:32.46246	24:54.17898	-1202	09/05/2018	15:29:19	2.7	335	rising	A
mo5	122:35.46742	25:03.47854	-1370	11/05/2018	01:16:31	7.9	576	low tide	A
m06	122:35.10787	25:03.64018	-1267	11/05/2018	01:21:46	7.9	635	low tide	A
m07	122:34.84143	25:03.70536	-1235	11/05/2018	01:24:13	7.9	410	low tide	A